Motions of an α-Helical Polypeptide: Comparison of Molecular and Harmonic Dynamics

D. PERAHIA,[1] R. M. LEVY[2] and M. KARPLUS[3]

[1]Laboratoire d'Enzymologie Physico-Chimique et Moléculaire, Bat 430, Université de Paris-Sud, 91405 Orsay, France; [2]Department of Chemistry, Rutgers, The State University of New Jersey, New Brunswick, New Jersey 08903, USA [3]Department of Chemistry, Harvard University, Cambridge, Massachusetts 02138, USA, and Laboratoire de Chimie des Interactions Moléculaires, Collège de France, 75005 Paris, France

SYNOPSIS

Molecular and harmonic dynamics simulations have been performed for a decaglycine α-helix. The extent of anharmonicity for various observables is studied by a direct comparison of the two types of simulations, at temperatures ranging from 5 to 300 K. The fluctuations of the cartesian, internal and normal mode coordinates, and their time dependence, are analyzed. The heat capacity of the α-helix is evaluated both from the temperature response of the system to an energy perturbation and from the fluctuations in the temperature of the system. It is shown that the anharmonicity depends on the kind of observable. The root mean square atomic fluctuations have significant anharmonic components at temperatures above 100 K. In contrast, the dihedral angle fluctuations are much closer to being harmonic at all the temperatures considered. The analysis of potentials of mean force experienced by individual atoms shows that atomic displacements have approximately Gaussian distributions from 50 to 300 K, with different force constants at each temperature (quasi-harmonic model). At 300 K, the force constants obtained by molecular dynamics are significantly lower than in the harmonic case. The time dependence of the projection of the molecular dynamics displacements on the normal mode coordinates shows that mode mixing is important above 100 K. The motions of the helix associated with the low-frequency normal modes are described and illustrated.

INTRODUCTION

A wide range of experimental and theoretical studies have shown the existence of internal motions in proteins.[1,2] Of particular importance have been molecular dynamics simulations, which have demonstrated that the root mean square (rms) of atom displacements in proteins are on the order of 0.5 Å, with a range of 0.1–2 Å,[1,3,4] a magnitude in overall agreement with estimates from x-ray diffraction and Mossbauer studies of protein crystals.[5-7] Further, molecular dynamics analysis of the time scales of the atomic fluctuations have indicated that they have a local subpicosecond component superposed on a larger scale more collective motion that develops over 1–10 or more picoseconds.[8,9] Two extreme models for such condensed-phase dynamic behavior can be formulated.[10] In the first, analogous to a liquid, the atomic fluctuations can be described as localized diffusion in which the collisions between atoms play the essential role; in the second, analogous to a solid, the atomic fluctuations involve the coupling of a large number of normal modes. It is likely that the interiors of proteins contain both fluid-like and

CCC 0006-3525/90/040645-33 $04.00
Biopolymers, Vol. 29, 645–677 (1990)

solid-like regions[5,10,11]; e.g., it has been suggested that hydrophobic clusters are more fluid-like, whereas parts with considerable secondary structure (α-helices, β-sheets) are more solid-like.[10] Results on the collective character of the motions indicate that the harmonic model may be useful for analysis, even if anharmonic contributions are present. Further, it has been suggested that the harmonic model may be improved by the quasi-harmonic approximation, in which the force constants are obtained not by differentiating the static potential energy function, but by averaging over the potential of mean force at a given temperature.[12-14]

In this paper we present the detailed results of a study of the full molecular dynamics of an isolated α-helix performed at a series of temperatures (5–300 K). The results are compared with those for the same system in the harmonic approximation.[15-18] The magnitudes of the atomic fluctuations and their time dependence are analyzed. Also, the potentials of mean force seen by the individual atoms at the various temperatures are calculated. The magnitudes and the time correlation functions of the fluctuations in cartesian and internal coordinates are compared with the corresponding harmonic dynamics results. The contributions of dephasing and population relaxation to the form of the correlation functions are examined. The heat capacity of the α-helix is evaluated both from the temperature response of the system to an energy perturbation and from the fluctuations in the temperature of the system. The motions of the helix associated with the low-frequency normal modes are described.

METHODOLOGY

The system considered is the model α-helix decaglycine, with the amino and carboxyl ends blocked by the CH_3CO and $NHCH_3$ groups, respectively; the decaglycine helix contains eight hydrogen bonds. All atoms and degrees of freedom of the molecule are treated explicitly, except that the CH_2 and CH_3 groups are represented as extended atoms. The details of the molecular model and the potential functions used in the present simulation have been presented previously.[15] A series of temperatures between 5 and 300 K defined by the mean kinetic energy of the system were studied. For each temperature, 20 trajectories, each 1 ps in length, were calculated by solving simultaneously the classical equations of motions for the atoms of which the helix is composed. Up to and including 100 K (5, 50, and 100 K), a kinetic energy twice the final desired temperature was imparted to the system in a single step; in all cases the temperature dropped to its mean value within 50–100 steps. At temperatures above 100 K, the system was heated 25–50 K every 200 steps until the desired temperature was reached. The total kinetic energy imparted to the system for the 20 trajectories with a given temperature was the same. The values of the average temperature of individual trajectories varied by up to 20%. In all cases, the initial coordinates for the system corresponded to the minimum energy geometry of the decaglycine helix and the individual trajectories of a set differed only in the initial velocity components chosen by using a set of random numbers corresponding to the appropriate Maxwellian distribution. Once the final temperature was reached in each case, the analysis of the trajectory was begun.

Twenty short trajectories with different initial conditions were used in an attempt to cover a larger portion of phase space than would a single extended trajectory in this relatively harmonic system. A set of 20 trajectories was chosen after a series of test calculations performed at 5 K in which the system was expected to be harmonic. It was found that this number gave consistent results when repeated with a different distribution of initial velocities. Sets of 5–10 trajectories showed deviation between different samples that were too large. We found that the differences between the rms displacements of the C_α atoms of the helix between sets of 5 trajectories at 5 K were about 0.005 Å, which represents almost 10% of the rms value at this temperature. Similar deviations were found with sets of 10 trajectories. The difference decreased to 0.001 Å when two sets of 20 trajectories were compared. In addition, a single longer trajectory was calculated at 300 K; it was equilibrated for 9 ps and the analysis period lasted 10 ps. The numerical integration of the equations of motions was carried out with the Verlet algorithm[19] with a time step of $5 \cdot 10^{-16}$ s. The program CHARMM[20] was employed for all of the computations.

The mean square amplitude of the fluctuations of a given atom, $\langle \Delta r^2 \rangle_D$, along the direction D, is evaluated by

$$\langle \Delta r^2 \rangle_D = \frac{\sum_{I=1}^{n} \langle (r_{ID} - \langle r \rangle_D)^2 \rangle}{n} \qquad (1)$$

in which r_{ID} is the projection of the instantaneous coordinate of the atom in the Ith trajectory onto the D direction and n is the number of trajectories in the set; the angle brackets represent time averages over individual trajectories and $\langle r \rangle_D = (\sum_{I=1}^{n} \langle r_{ID} \rangle)/n$ is the mean value of the displacement in the D direction for the 20 trajectories.

The harmonic approximation to the amplitudes of atomic vibrations are obtained from the eigenvalues and eigenvectors of the decaglycine α-helix[15]; that is

$$\langle \Delta r^2 \rangle_{D\text{har}} = k_B T \sum_{j=1}^{3N-6} \frac{\alpha_{jD}^2}{\omega_j^2} \qquad (2)$$

in which k_B is the Boltzmann constant, T is the absolute temperature, N is the number of atoms, ω_j is the frequency of the jth normal mode, and α_{jD} is the component of the jth eigenvector along D direction for the atom of interest. To obtain the normal modes, the energy of the α-helix was minimized by using the full potential, and the second-derivative matrix of the potential energy with respect to the mass-weighted cartesian coordinate displacements relative to the minimal-energy structure was determined. Details concerning the harmonic dynamics method as applied to the α-helix have been reported.[15]

The second moment and normalized third and fourth moments of the displacements of a given atom were computed along the principal axes of motion. The axes were obtained by the diagonalization of the cartesian mean square displacement matrix corresponding to the atom.[21] The moments give an indication of the nature and extent of the anharmonicity.

The "normalized" third (skewness) and fourth (kurtosis) moments are defined by

$$\langle \Delta r^3 \rangle_{DN} = \frac{\langle \Delta r^3 \rangle_D}{\langle \Delta r^2 \rangle_D^{1/2}}, \qquad \langle \Delta r^4 \rangle_{DN} = \frac{\langle \Delta r^4 \rangle_D}{\langle \Delta r^2 \rangle_D^2} - 3 \qquad (3)$$

where Δr is the displacement of the atom relative to the mean position and N indicates that the moment is normalized; both $\langle \Delta r^3 \rangle_{DN}$ and $\langle \Delta r^4 \rangle_{DN}$ are equal to 0 for a harmonic system.

To determine the time dependence of the positional fluctuation, the normalized autocorrelation function

$$C(\vec{\Delta r}) = \frac{\langle \vec{\Delta r}(0) \cdot \vec{\Delta r}(t) \rangle}{\langle \vec{\Delta r}(0)^2 \rangle} \qquad (4)$$

was evaluated. The components of this function along given directions were also considered. In the harmonic case, the time correlation function of positional fluctuations was evaluated by the equation

$$\langle \vec{\Delta r}(0) \cdot \vec{\Delta r}(t) \rangle_{\text{har}} = \frac{k_B T \sum_{j=1}^{3N-6} \alpha_j^2 \cos(\omega_j t)}{\omega_j^2} \qquad (5)$$

Spectral densities corresponding to the variation of a given variable in the molecular dynamics simulation were obtained by taking the Fourier transform of its autocorrelation function. The fast Fourier transform technique was used for these calculations.[22] In the harmonic case, the spectral densities were obtained by considering the contribution of normal modes to the mean square fluctuation of the given variable.

RESULTS AND DISCUSSION

In this section we present and discuss the results. We emphasize the calculations at 300 K, where both 20 short and 1 long trajectory are available for comparison, and consider the lower temperature calculations only as appropriate.

Anisotropy of Atomic Displacements

To examine the anisotropy of the atomic motions, the rms fluctuations for individual atoms have been computed along different directions; we present the results from the 20 1-ps trajectories and the 10-ps trajectory at 300 K. For each atom three directions are defined relative to the energy-minimized structure: one is parallel to the helix axis (axial vector **A**); the second is perpendicular to the axial vector and is within the plane including the axial vector and the atom of interest (radial vector **R**); and the third is perpendicular to the axial and radial vectors (tangential vector **T**). The rms amplitudes of the fluctuations computed for each atom type in these three directions from molecular dynamics [Eq. (1)] and harmonic analysis [Eq. (2)] at 300 K are summarized in Table I; as indicated, only the internal residues (2–10) are included in the average. In Fig. 1 we present the magnitudes of the fluctuations for the N atom as a function of

Table I Atom Type RMS Fluctuations Along Helix Directions at 300 K by Molecular and Harmonic Dynamics[a]

Atom	Molecular Dynamics			Harmonic Dynamics		
	Axial	Tangential	Radial	Axial	Tangential	Radial
C_α	0.27	0.48	0.28	0.17	0.34	0.18
N	0.22	0.39	0.28	0.11	0.26	0.21
C	0.23	0.39	0.26	0.11	0.26	0.17
O	0.29	0.45	0.40	0.14	0.33	0.30
H	0.23	0.42	0.42	0.12	0.33	0.41

[a]All values in Å for atoms of a given type averaged over residues 2–10. The 20 1-ps short trajectories were employed for the molecular dynamics values.

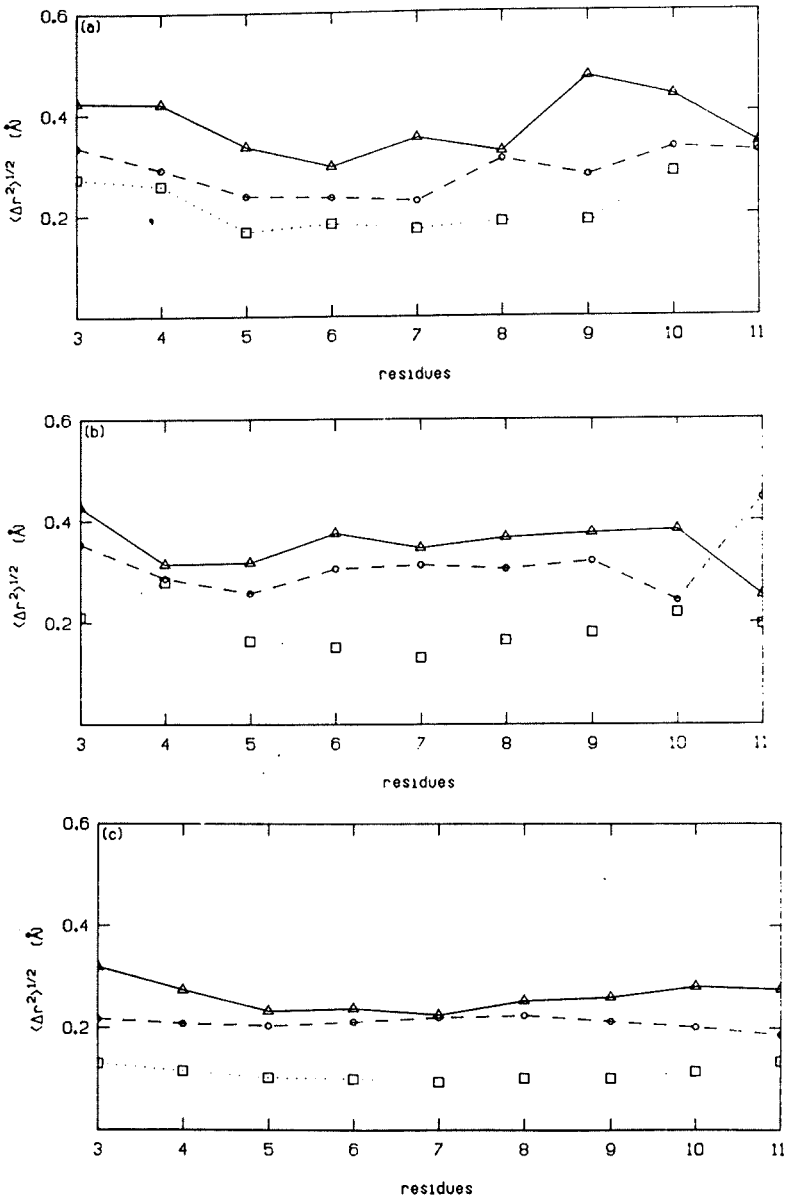

Figure 1. Root mean square atomic displacements of atom N as a function of residue number along the helix directions, obtained from (a) 20 1-ps molecular dynamics trajectories, (b) 10-ps molecular dynamics trajectory, and (c) harmonic dynamics. Full curve corresponds to tangential, dashed curve to radial, and dotted curve to axial directions.

Table II RMS Fluctuations for the Atom Types Along Principal Axes of Motion at 300 K from Molecular Dynamics[a]

Atom	Largest Fluctuation	Second Largest Fluctuation	Smallest Fluctuation
C_α	0.53	0.27	0.21
N	0.43	0.26	0.16
C	0.44	0.24	0.16
O	0.50	0.39	0.18
H	0.47	0.40	0.17

[a]All values in Å for atoms of a given type averaged over residues 2–10. The 20 1-ps short trajectories were employed.

residue number, obtained from the 10-ps, the 20 1-ps trajectories and the harmonic dynamics. For the heavy atoms the magnitudes of fluctuations along the tangential directions are generally the largest and the axial fluctuations are generally the smallest. This is true for both molecular and harmonic dynamics. Such an anisotropy suggests that, at least for a helix of this size, the twisting motions are more important than bending and stretching motions. For hydrogen atoms, the fluctuations along the tangential and radial directions are of similar magnitude in molecular dynamics, while in harmonic dynamics, the radial displacements are more important than the tangential ones. The fluctuations along tangential and radial directions of N and O atoms are close to each other in harmonic dynamics; the differences are larger in molecular dynamics. The rms displacements per type of atom along the backbone are slightly more regular in the harmonic results, although the variations from one residue to another in the molecular dynamics results are not very great. However, the 10-ps molecular dynamics results are somewhat more regular than the 20 1-ps results. This suggests that a larger set of short trajectories is needed to have a complete representation of the motions. The fluctuations along the principal axes of displacement for each atom type are summarized in Table II. These directions correspond to the eigenvectors of the matrix whose diagonal elements are the mean square fluctuations along the three coordinate axes ($\langle \Delta x^2 \rangle$, $\langle \Delta y^2 \rangle$, $\langle \Delta z^2 \rangle$), and whose off-diagonal elements are the cross terms between these fluctuations ($\langle \Delta x \Delta y \rangle$, $\langle \Delta x \Delta z \rangle$, etc.); the eigenvalues correspond to the mean square fluctuations along the principal axes. The results show that, in general, the motion of atoms within the helix are significantly anisotropic. The ratio between the largest and smallest principal components of the rms fluctuations is about 2, with the anisotropy increasing toward the two ends of the helix.

It is instructive to examine the relation between the principal axes directions of displacement of each atom and the helix directions. For N, C, C_α, and O atoms, the eigenvectors with the largest eigenvalue have, to a large extent, the same orientation as the tangential directions. For H atoms the eigenvector having the largest eigenvalue corresponds to the tangential and radial directions, alternating from one residue to the next. The eigenvectors having the second largest eigenvalue for N, C, and O atoms correspond to the radial directions. However, for the C_α atoms, they correspond to radial and axial directions alternatively from one residue to the next; for H atoms, they again alternate between the tangential and radial directions.

Anharmonicity of Atomic Displacements

Mean Square Displacements

The effective anharmonicity of the atomic motions may be estimated by comparing the molecular and harmonic dynamic values of the mean square displacements at different temperatures. It was shown previously[12] for the same α-helical model that up to 50 K the harmonic rms values obtained for all the atomic displacements are very close to corresponding molecular dynamics values. The difference between the two methods becomes significant at 100 K, with a ratio of 1.74 between mean square values for C_α atoms, and it increases to a ratio of 2.45 at 300 K. The anharmonicity for the 20 trajectories at 300 K was found to be introduced by the dispersion of the mean structures corresponding to each 1-ps trajectory. The local high-frequency (1-ps) fluctuations around a given mean structure were close to those obtained from a harmonic model. The analysis of the 20 1-ps trajectories was confirmed by the fact that the 10-ps trajectory at 300

K yielded very similar rms values. This suggested that harmonic dynamics was adequate for studying structural fluctuations of an α-helix up to 50 K, but that a molecular dynamics simulation was required for higher temperatures.

It is of interest to compare the calculated C_α atom rms fluctuations for the decaglycine helix and the experimental estimates from x-ray temperature factors for the helices in metmyoglobin at various temperatures.[5,23] The metmyoglobin values are close to those calculated for the central residues of decaglycine by molecular dynamics; i.e., 0.28, 0.41 and 0.48 Å at 80, 250, and 300 K for metmyoglobin, respectively, as compared with 0.20, 0.42, and 0.52 Å from the isolated helix simulations at the same temperatures, respectively (the 80 K theoretical rms value is deduced by a linear interpolation between the mean square displacements at 50 and 100 K).

The anharmonic contributions to the various components of the fluctuations are different at 300 K (see Table I). The rms displacements in the molecular dynamics along the axial direction are about twice the corresponding harmonic values; this ratio is around 1.4 for the tangential direction, and between 1 and 1.5 for the radial direction. The two types of trajectories (10 and 20 1-ps) give similar results concerning the anharmonicity for the N atoms [Fig. 1(a and b)].

The extent of the anharmonicity for the mean square displacements along the helix directions at different temperatures are shown in Fig. 2 for the C_α atom of the sixth residue. The molecular dynamics displacements along the tangential direction vary almost linearly with temperature between 50 and 300 K. However, the corresponding harmonic quantities are significantly smaller, indicating that anharmonic effects are present. For the axial direction, the mean square displacement of the C_α atom is close to the corresponding harmonic mean square displacement up to a temperature of 200 K, but increases rapidly from 200 to 300 K. This amplification of the axial motion at higher temperatures involves a variation in the length of the hydrogen bonds. The molecular dynamics radial mean square displacements are close to the harmonic values for the entire temperature range. Mossbauer spectroscopy[24,25] measurements of the temperature (Debye-Waller) factor for ^{57}Fe in myoglobin as a function of temperature suggest that at approximately 200 K there is a transition leading to increased motion in the interior. From the present study it appears that part of the observed increase is due to the greater anharmonic contributions to the motion above 200 K.

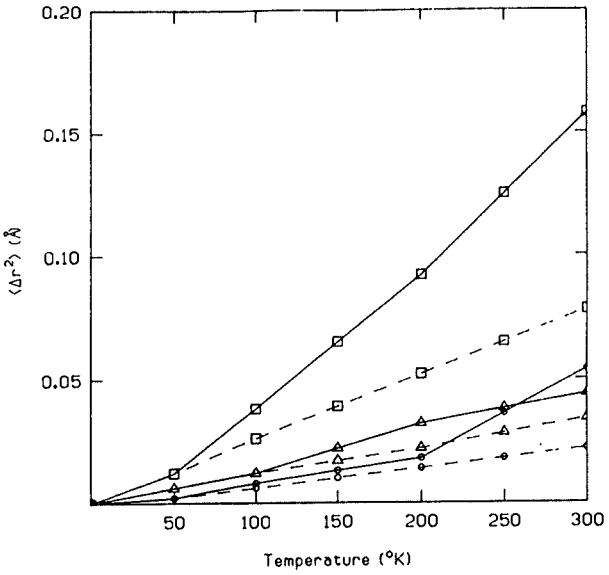

Figure 2. Temperature dependence of mean square atomic displacements obtained by molecular dynamics and harmonic analysis for the C_α atom of the sixth residue along its helix directions. Squares correspond to the tangential, triangles to the radial, and circles to the axial directions. Full lines correspond to molecular dynamics and dashed lines to harmonic case.

The temperature dependence of the rms fluctuations and its deviations from harmonic behavior can be interpreted in terms of two different models. One is a temperature-independent anharmonic oscillator model where the potential has cubic, quartic, and higher terms. An alternative model assumes that the potential is quadratic with respect to displacements, but that the force constants are temperature dependent and can be estimated from molecular dynamics or Monte Carlo simulations[14,26]. In this quasi-harmonic model, anharmonic effects are implicitly taken into account by the values of temperature-dependent force constants. There is, of course the possibility that neither of these models, which basically involve perturbation treatments of the harmonic problem, are generally valid. Molecular dynamics simulations, particularly for side chains, have shown that in some cases multiwell potentials play an important role.[27] We also note that the dependence of the mean square displacements of individual atoms on the absolute temperature T in the x-ray studies of metmyoglobin[5] has been described analytically by T^μ, in which μ ranges from -2 to 20 depending on the local environment of atoms; only few residues seemed to have harmonic potentials for which $\mu = 2$.

Table III Quasi Harmonic and Harmonic Force Constants for the C_α Atom of the Sixth Residue of α-Helix at Different Temperatures Derived from Molecular Dynamics Trajectories

Temperature (K)	Force Constants (kcal/mol-Å)		
	Axial	Tangential	Radial
50	31.0	8.2	16.8
100	26.4	5.2	18.0
200	21.0	4.4	12.4
300	10.8	3.8	13.2
Harmonic	26.0	7.4	16.6

Since the distribution of displacements for the α-helix is found to be nearly gaussian at 50 and 300 K (see below), the effective potential for the positional fluctuation (quasiharmonic approximation) may be approximated by $V = \frac{1}{2}k\Delta r^2$ at each temperature, with different values of k as a function of temperature. We estimate the force constants for the displacements of the C_α atom of the sixth residue by the equation

$$k_D = \frac{k_B T}{\langle \Delta r^2 \rangle_D} \tag{6}$$

for the various helix directions D. The resulting values for the force constants are shown in Table III. At 50 K, the molecular dynamics force constants along all three of the local helix directions are somewhat larger than the harmonic values; at 100 K the tangential molecular dynamics force constant is significantly smaller, while the axial and radial molecular dynamics force constants are very close to the corresponding harmonic results. In accord with Fig. 2, the decrease of the molecular dynamics force constants along the axial direction with increasing temperature is most important (a factor 3 from 50 to 300 K); the corresponding decreases along the radial and tangential directions are also significant, although less important.

Higher Moments

We present in Table IV the mean absolute values of the skewness [eq. (3)] per atom type along the principal axes of motion, at 50 and 300 K, respectively. As expected, the values corresponding to 50 K are in general smaller than for 300 K. Figure 3(a and b) give the values at the two temperatures for the N atoms as a function of residue number. At 300 K, the largest anharmonicities are observed in most cases for terminal residues; this behavior is less marked at 50 K. The H atoms are less skewed (smaller third moment) than the other atoms. There is no apparent rule about the magnitude of

Table IV Skewness and Kurtosis for Atom Types Along Principal Axes of Motion at 300 K by Molecular Dynamics[a]

Temperature	Atom	$\lvert\langle \Delta x^3 \rangle_N\rvert$			$\lvert\langle \Delta x^4 \rangle_N\rvert$		
		Largest	Second Largest	Smallest	Largest	Second Largest	Smallest
50	C_α	0.25	0.15	0.15	0.25	0.62	0.36
	N	0.22	0.20	0.10	0.40	0.41	0.33
	C	0.24	0.10	0.13	0.40	0.55	0.58
	O	0.26	0.14	0.10	0.24	0.38	0.30
	H	0.08	0.18	0.09	0.16	0.18	0.36
300	C_α	0.31	0.35	0.33	0.34	0.27	0.42
	N	0.28	0.24	0.24	0.36	0.31	0.34
	C	0.28	0.37	0.30	0.33	0.48	0.48
	O	0.29	0.30	0.40	0.35	0.35	0.34
	H	0.24	0.25	0.30	0.39	0.26	0.31

[a]Averages of absolute values are over residues 1–11. The 20 1-ps short trajectories were employed. The terms largest, second largest, and smallest refer to the principal axes direction having the largest, second largest, and smallest $\langle \Delta x^2 \rangle$ eigenvalues.

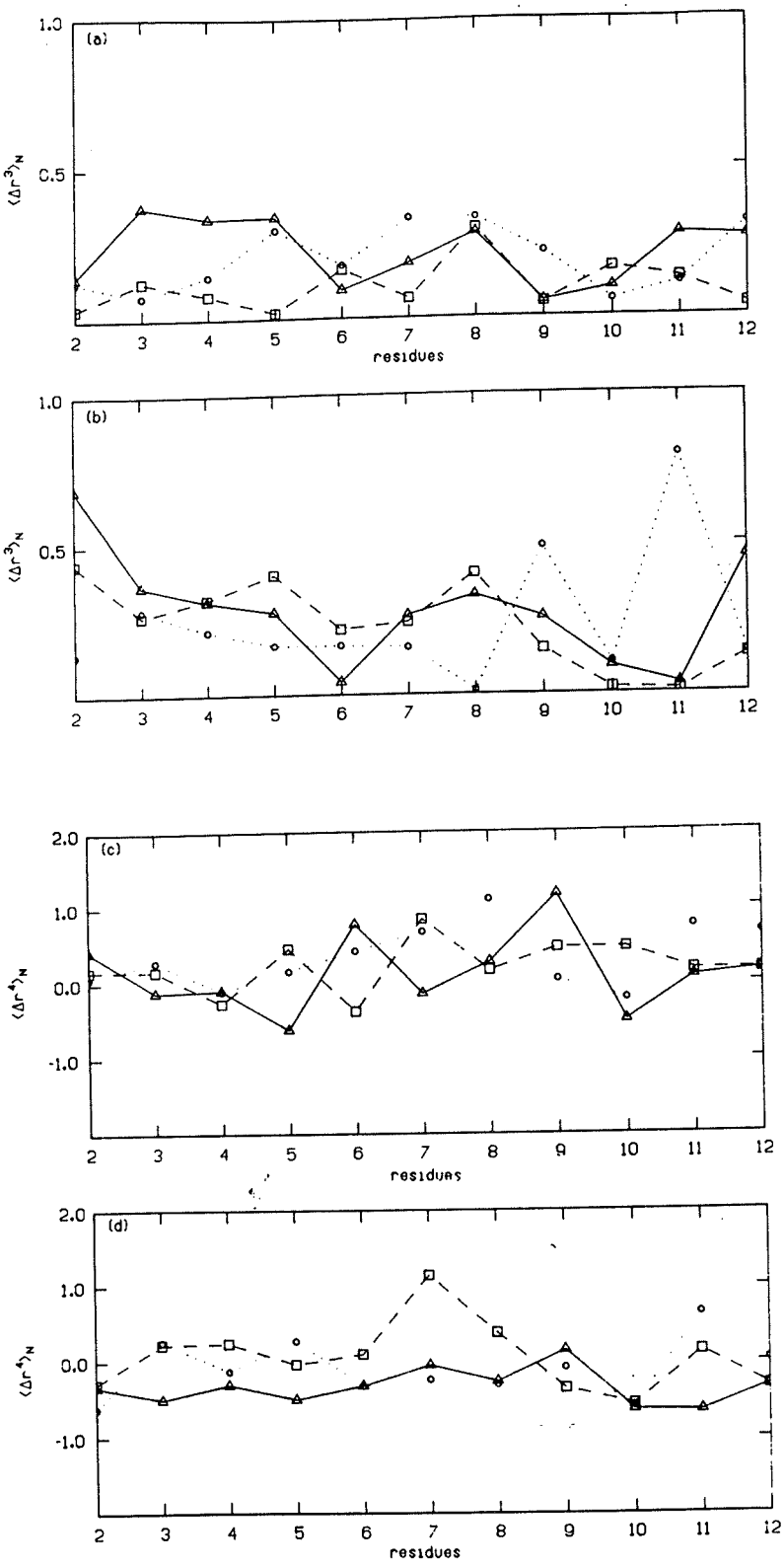

Figure 3. Third and fourth moments of atomic displacements along the principal axes of motion, for atom N, as a function of residue number, obtained from 20 1-ps molecular dynamics trajectories, at two temperatures. (a) Absolute normalized third moments at 50 K, (b) absolute normalized third moments at 300 K, (c) normalized fourth moments at 50 K, and (d) normalized fourth moments at 300 K. Full curve corresponds to largest eigenvalue, dotted curve to second largest eigenvalue, and dashed curve to smallest eigenvalue.

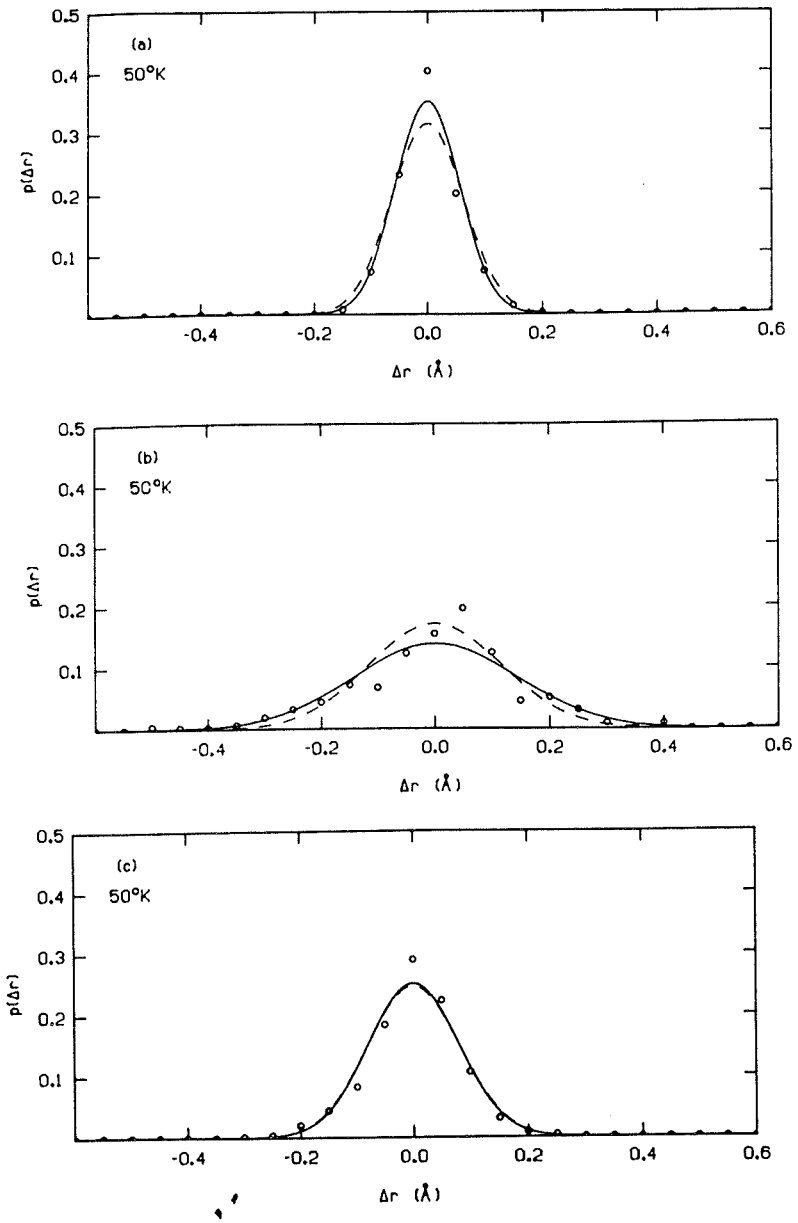

Figure 4. Probabilities of occurrence of cartesian displacements of the C_α atom of the sixth residue along the helix directions, obtained at three temperatures from 20 1-ps molecular dynamics trajectories. (a) 50 K axial, (b) 50 K tangential, (c) 50 K radial, (d) 100 K axial, (e) 100 K tangential, (f) 100 K radial, (g) 300 K axial, (h) 300 K tangential, (i) 300 K radial. Circles correspond to molecular dynamics, full line to quasi-harmonic approximation to molecular dynamics, and dashed line to harmonic dynamics.

the third moment as far as which principal axis is most important.

As for the kurtosis, the mean absolute values per atom type are also given for 50 and 300 K in Table IV. Figure 3(c and d) show the N atom values as a function of residue number. The C_α, C, O, and N atoms show larger absolute values, in general, than H atoms. The fourth moments are especially large toward the ends of the helix at 300 K. At 50 K, the majority of values observed are positive, while at 300 K a large number of values, particularly those corresponding to the principal axes having the largest eigenvalue, have negative values. In fact, 86% of atoms have a negative kurtosis for the fluctuations along their principal axes corresponding to the largest eigenvalue. For the second largest

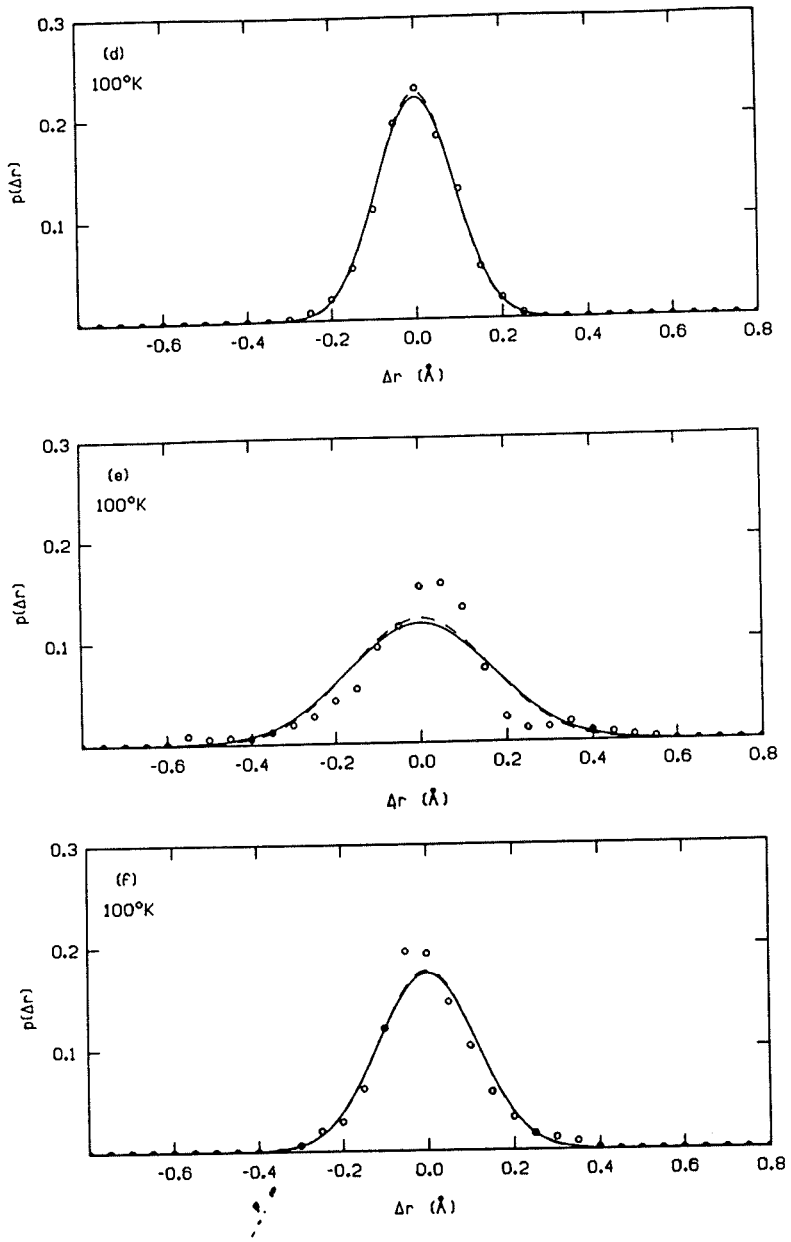

Figure 4. *(Continued from the previous page.)*

eigenvalue, 61% of atoms have a negative kurtosis; this proportion goes down to 25% for the lowest eigenvalue. A negative kurtosis implies that the distribution is more peaked and the wings are depleted compared to a gaussian distribution. This means that the effective potential wells are steeper than the corresponding harmonic wells.

Examining the relations among the various moments we find that large positive values of the fourth moment are obtained for large absolute values of the third moment, and negative values of the fourth moment are obtained for small absolute values of the third moment. Also, large positive values for the fourth moment are obtained for small values of the second moment. Similar correlations between the values of the third and fourth moments, and between the second and fourth moments, are reported in the study of anharmonicity of atomic displacements in cytochrome C[21] and lysozyme[27] molecular dynamics simulations at 300 K. The similarity of the results obtained for the different molecular systems emphasizes the general character of these correlations. However, although anharmonicity measurements have been made in

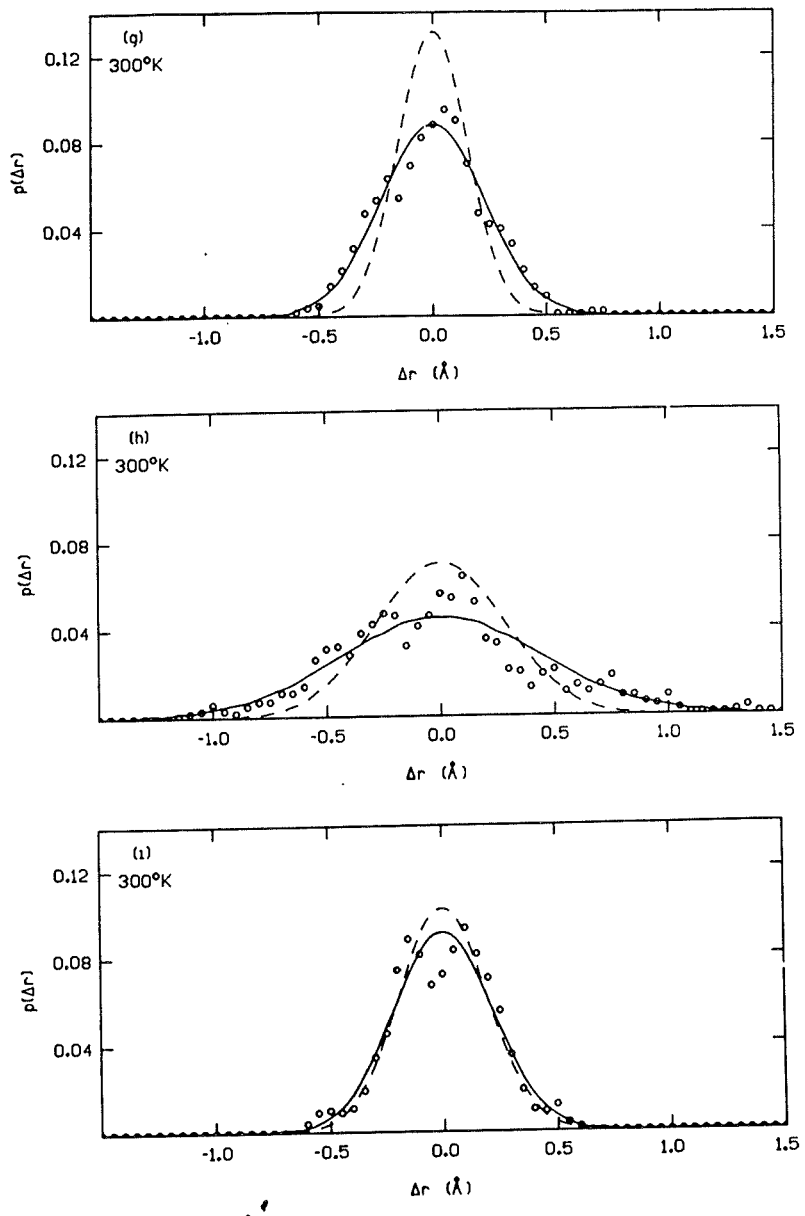

Figure 4. *(Continued from the previous page.)*

small molecule crystals, available protein x-ray results are not at high enough resolution to make such an analysis possible.

Position Probability Distribution and Potentials of Mean Force

The probability $p(\Delta r)_D$ of finding the displacement Δr from the mean position in the direction D of a given atom has been evaluated. These probabilities were obtained from the molecular dynamics trajectories by taking the ratio of the number of times that Δr appears in a given interval and the total number of points in the trajectories. Intervals of 0.05 Å were used. The directions D correspond to the helix directions.

For comparison, the probabilities in the harmonic and quasi-harmonic approximations were also computed. The probability density of a classical oscillator in thermodynamic equilibrium at a given temperature is given by

$$p(\Delta r)_D = \frac{\exp\left[(-\Delta r^2)/\langle \Delta r^2 \rangle_D\right]}{\sqrt{2\pi \langle \Delta r^2 \rangle_D}} \qquad (7)$$

where $\langle \Delta r^2 \rangle_D$ is the harmonic mean square displacement of the atom of interest in the direction D at the temperature considered. The probabilities of occurrence of different displacements within the intervals (the same as in the corresponding molecular dynamics case) are obtained by integrating $\rho \langle \Delta r \rangle_D$ over these intervals. The probabilities in the quasi-harmonic approximation are obtained from a gaussian distribution with the variance equal to the second moments of the molecular dynamics displacements.

The positional probability distributions along helix directions at 50, 100 and 300 K for the C_α atom of the sixth residue are presented in Fig. 4. At 50 K the harmonic probabilities are close to the gaussian fit of the molecular dynamics probabilities, although the molecular dynamics probabilities show some positive skewness along the tangential direction. At 100 K the molecular dynamics and harmonic probability distributions along the axial and radial directions are very similar. Along the tangential direction, however, the molecular dynamics probability distribution is more highly peaked than the harmonic probability distribution (negative kurtosis), while the quasi-harmonic result remains close to the harmonic distribution. At 300 K [Fig. 4(g, h, i)] the molecular dynamics probability distributions are irregular in shape and underpopulated in the neighborhood of the mean as compared with the harmonic distribution. The molecular dynamics probability distribution is closer to the harmonic distribution in the radial than in the axial and tangential directions. Overall, the quasiharmonic approximation is excellent in the radial direction, and adequate for some purposes in the axial and tangential directions. However, it is clear that at least part of the temperature dependence arises from aspects of the dynamics that cannot be represented in a quasi-harmonic form.

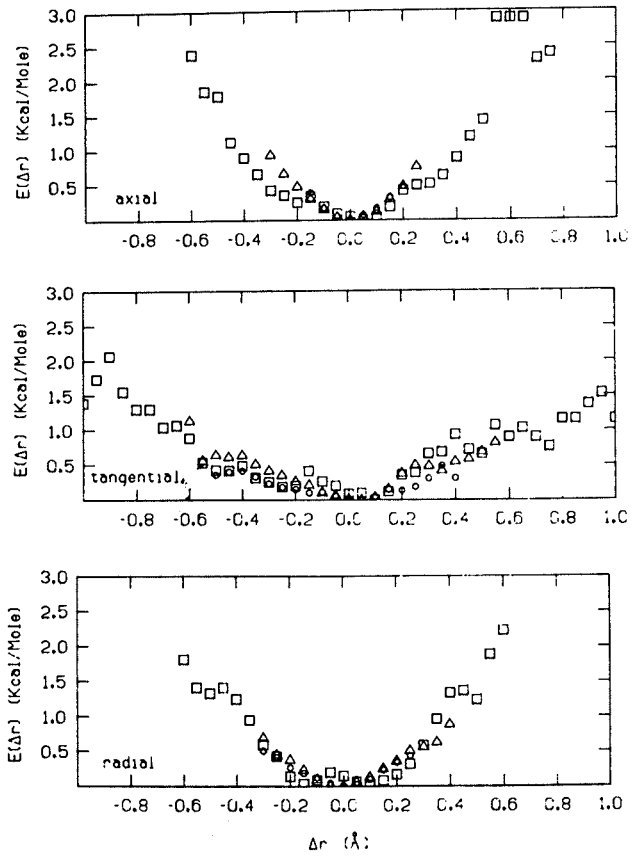

Figure 5. Potential of mean force corresponding to cartesian diaplacements of C_α atom of the sixth residue along the helix directions at various temperatures, obtained from 20 1-ps molecular dynamics trajectories. Circles correspond to 50 K, deltas to 100 K, and squares to 300 K.

An alternative to the probability distributions is given by the potential of mean force. It is evaluated for a given temperature from the equation $E(\Delta r)_D = -RT \ln \rho(\Delta r)_D$. Figure 5 shows the potentials of mean force corresponding to displacements along the axial, tangential, and radial directions of the C_α atom of the sixth residue at temperatures of 50, 100, and 300 K. The potentials at different temperatures remain relatively similar to each other, and in all cases, approximate a harmonic well.

The analysis of the probability distributions provides evidence both for a variation of the force constant with temperature and anharmonic effects at a single temperature. However, the results justify the use of a temperature-dependent force constant and harmonic potentials as the first approximation to the probability distributions of the atoms in the α-helix.

Time Dependence

The autocorrelations of the displacements for the C_α atom of the sixth residue calculated by use of Eqs. (4) and (5), and from molecular dynamics and harmonic dynamics, are shown in Fig. 6. The molecular dynamics results correspond to the 10–ps trajectory at 300°K. In a previous article (Ref. 12, Fig. 3) the formula

$$C(|\overrightarrow{\Delta r}|) = \frac{\langle |\overrightarrow{\Delta r}(0)| \cdot |\overrightarrow{\Delta r}(t)| \rangle}{\langle |\overrightarrow{\Delta r}(0)|^2 \rangle} \tag{8}$$

was employed. It gives the autocorrelation function in the positional fluctuation without reference to directionality. Since $C(|\overrightarrow{\Delta r}|)$ decays much more slowly than $C(\overrightarrow{\Delta r})$ given in Eq. (4), the reorienta-

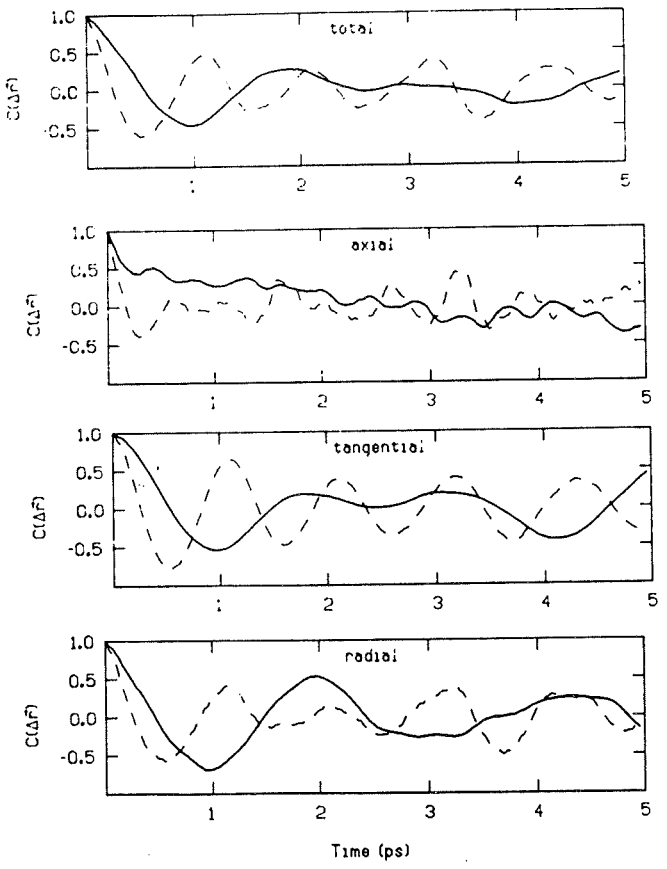

Figure 6. Normalized autocorrelation functions for the time dependence of the atomic displacements at 300 K of C_α atom of the sixth residue; the behavior of the total displacement vector and its components along the helix directions are shown. Full curves correspond to 10-ps molecular dynamics, and dashed curves to harmonic case.

tion of the vector plays an important role in the time dependence. The autocorrelation of the displacements of the same C_α atom along its local helix directions are also shown in this figure. The tangential and radial functions, as well as the total, show smooth oscillations with a slow overall decay (Fig. 6). By contrast, the axial function is more unstructured with significant higher frequency oscillations; these are due to the motion involving stretching of the hydrogen bonds. In general, the molecular dynamics and harmonic results are rather similar, although the dominant oscillation in the former are at lower frequencies than in the latter. To analyze the time dependence in more detail, the spectral densities of the autocorrelation functions are presented in Fig. 7; for the harmonic dynamics, the exact spectral densities are shown. Along the axial direction in the molecular dynamics results the dominant frequencies observed are around 12, 18 and 26 cm^{-1} (the peak around 4 cm^{-1} corresponds to the slow decay of the curve); in the harmonic case the main frequencies observed are around 21, 36, 41, 51, and 62 cm^{-1}. Along the tangential direction the frequencies involved are lower than in the axial direction; the main frequencies observed are around 12 and 21 cm^{-1} in molecular dynamics, and 23, 30, and 33 cm^{-1} in harmonic dynamics. In the radial direction, a large peak around 15 cm^{-1} is observed in molecular dynamics, and three main frequencies around 23, 30, and 33 cm^{-1} in harmonic dynamics. Thus, the harmonic and molecular dynamics spectra differ significantly.

Anharmonicity Along Normal Modes

The anharmonicity may also be studied by analyzing the atomic displacements in the direction of harmonic normal mode vectors. This permits one to examine directly the effect of mode mixing on

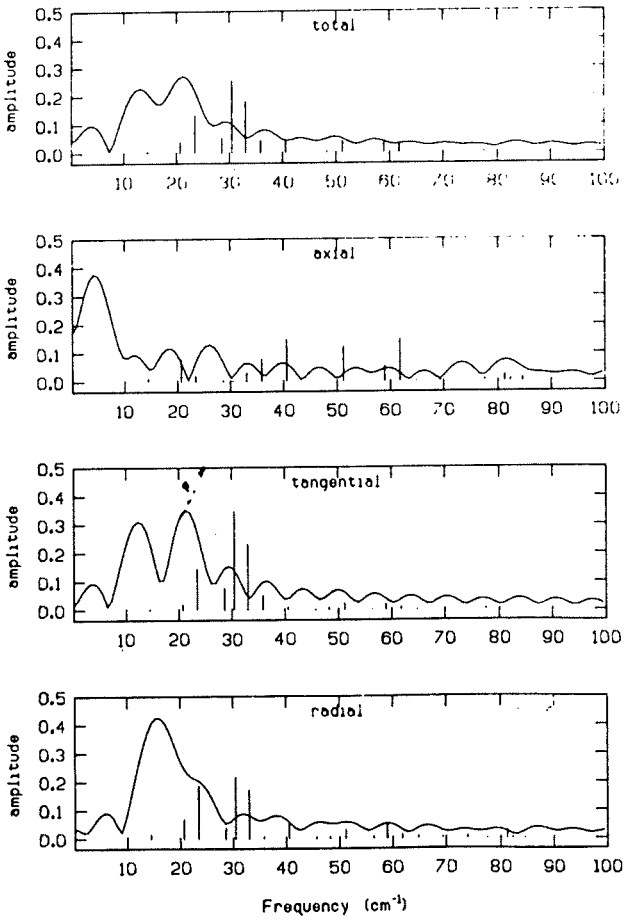

Figure 7. Spectral densities corresponding to the autocorrelation functions of Fig. 6. Curves correspond to 10-ps molecular dynamics, and bars to harmonic case.

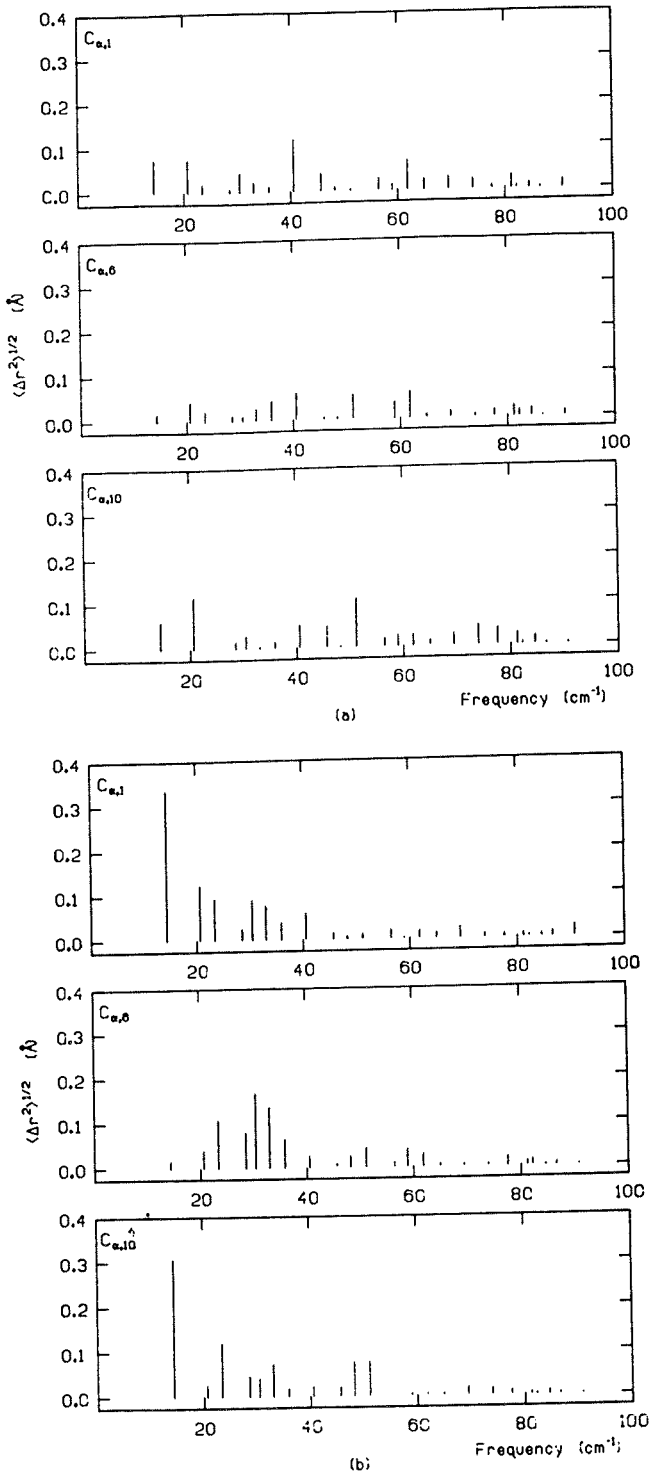

Figure 8. Spectral density of rms displacements of certain C_α atoms along the helix directions obtained by harmonic analysis. (a) Axial, (b) tangential, and (c) radial.

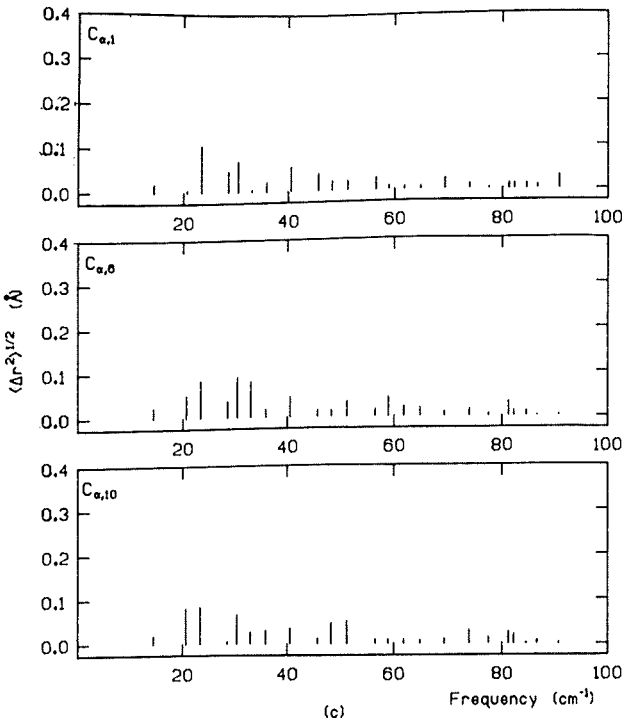

Figure 8. *(Continued from the previous page.)*

the fluctuations and their time dependence. We consider the following projection:

$$Q_j = \sum_k^N m_k^{1/2} \overrightarrow{\Delta r_k} \cdot \overrightarrow{\alpha_{jk}} \qquad (9)$$

where m_k is the atomic mass of atom k, $\overrightarrow{\Delta r_k}$ is the molecular dynamics instantaneous cartesian displacement vector with respect to the mean position of atom k and $\overrightarrow{\alpha_{jk}}$ is the component of the jth normal mode associated with atom k; the summation is over all the atoms. The Q_j have been computed for every step of the 20 1-ps trajectories.

Spectral Densities of Mean Square Atomic Displacements

To determine the modes making the most significant contributions to the atomic displacements, we first present the spectral densities of these displacements. In Fig. 8 we present the spectral densities of the rms displacements of some C_α atoms obtained by harmonic analysis, along the axial, tangential, and radial directions, respectively. Important contributions from the lowest frequency (14.4 cm^{-1}) are observed along the tangential direction for the terminal residues (C_α^1, C_α^{10}) [Fig 8(b)]. For the middle residues (C_α^6), the dominant frequencies are shifted to larger values; there are appreciable contributions from frequencies 23.4 and 30.5 cm^{-1}. As far as the axial and radial directions are concerned [Fig. 8 (a and c)] there is less difference between the central and end residues; only a slight shift to larger values of mean frequencies is observed toward the middle of the helix. In the axial direction [Fig. 8 (a)] the spectrum is more spread out (between 14.4 and 81.2 cm^{-1}) than in the case of the tangential and radial directions. In Fig. 9 we present the spectrum of rms displacements of N, C, C_α, O, and H atoms of the sixth residue, along the helix direction; it should be noted that the scale is different from Fig. 8. The spectral density of all these atoms along the tangential direction is centered around 30.5 cm^{-1}; O and H atoms show an appreciable spectral density between 50 and 100 cm^{-1}; the spectral density of the H atom extends to significantly larger frequencies (300 cm^{-1}). Along the radial direction, larger contributions are observed in the frequency domain beyond 50 cm^{-1}, as compared with tangential direction; for atom O the spectral density between 50 and 80 cm^{-1} is more important than up to 50 cm^{-1}; for N atom appreciable density is observed between 100 and 200 cm^{-1}; for H atom the spectral density between 100 and 300 cm^{-1} is particularly important. There is considerable similarity between the results for the bonded atoms N and H.

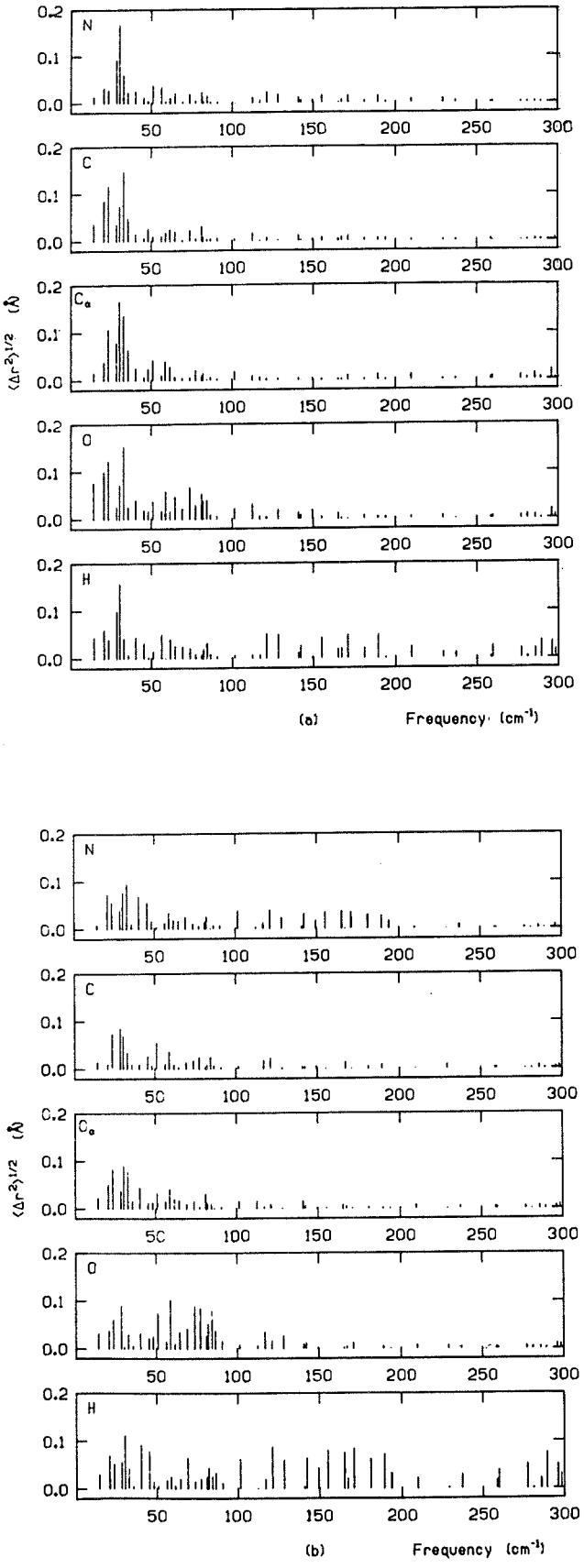

Figure 9. Spectral density of rms displacements of the atoms of the sixth residue along the helix directions from harmonic analysis. (a) Tangential, (b) radial, and (c) axial.

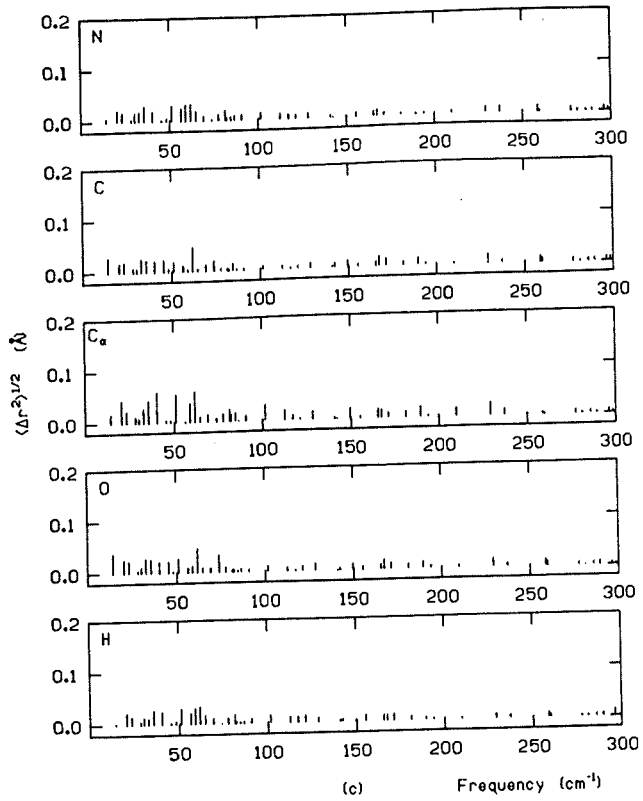

Figure 9. *(Continued from the previous page.)*

The normal mode distribution extending over a wide range of frequencies is generally consistent with inelastic neutron scattering data for helical biopolymers[28] such as α-poly-L-alanine.[29,30] However, a quantitative comparison would require calculations of the inelastic neutron scattering from the normal modes.[31]

Potential Energy Curves

The total potential energy was computed as a function of atomic displacements along a number of different normal modes. This is one way to determine the deviation from harmonic behavior. We have varied only the dihedral angles, keeping constant the bond lengths and bond angles, to avoid artificially high energies due to curvilinear effects. The results are presented in Fig. 10 for the modes with frequencies of 14.41, 23.45, 30.47, and 40.56 cm^{-1}; the harmonic potentials are included for comparison. Up to energies of about 5 kcal/mol, the harmonic and full potentials are close to each other for all frequencies presented. For larger energies, the full potentials are steeper than the harmonic potentials in all cases; for higher frequencies (here 40.56 cm^{-1}) the two curves deviate less. It is interesting to contrast the present results with the molecular dynamics displacements of C_α at 300 K. Figure 4(g, h, and i) show that the actual displacements are larger than those for the harmonic approximation, corresponding to a smaller value of the potential of mean force. This is due to the fact that in the molecular dynamics mode mixing occurs. For the energy along a mode, van der Waals collisions, which could be avoided if other modes were mixed in, raise the energy. It should be noted, however, that the region where anharmonic effects are important involves energies that are much larger than kT and so are not significantly sampled at 300 K or below.

Probability Distribution

The probability distributions of the normal mode coordinate projections Q_j, have been computed from the molecular dynamics in the same way as for the cartesian atomic displacements (see the previous section). The results correspond to the 20 1-ps trajectories at 50, 100, and 300 K. The displacements were computed with respect to the global average position for all the 20 1-ps trajectories. The averages corresponding to each 1-ps tra-

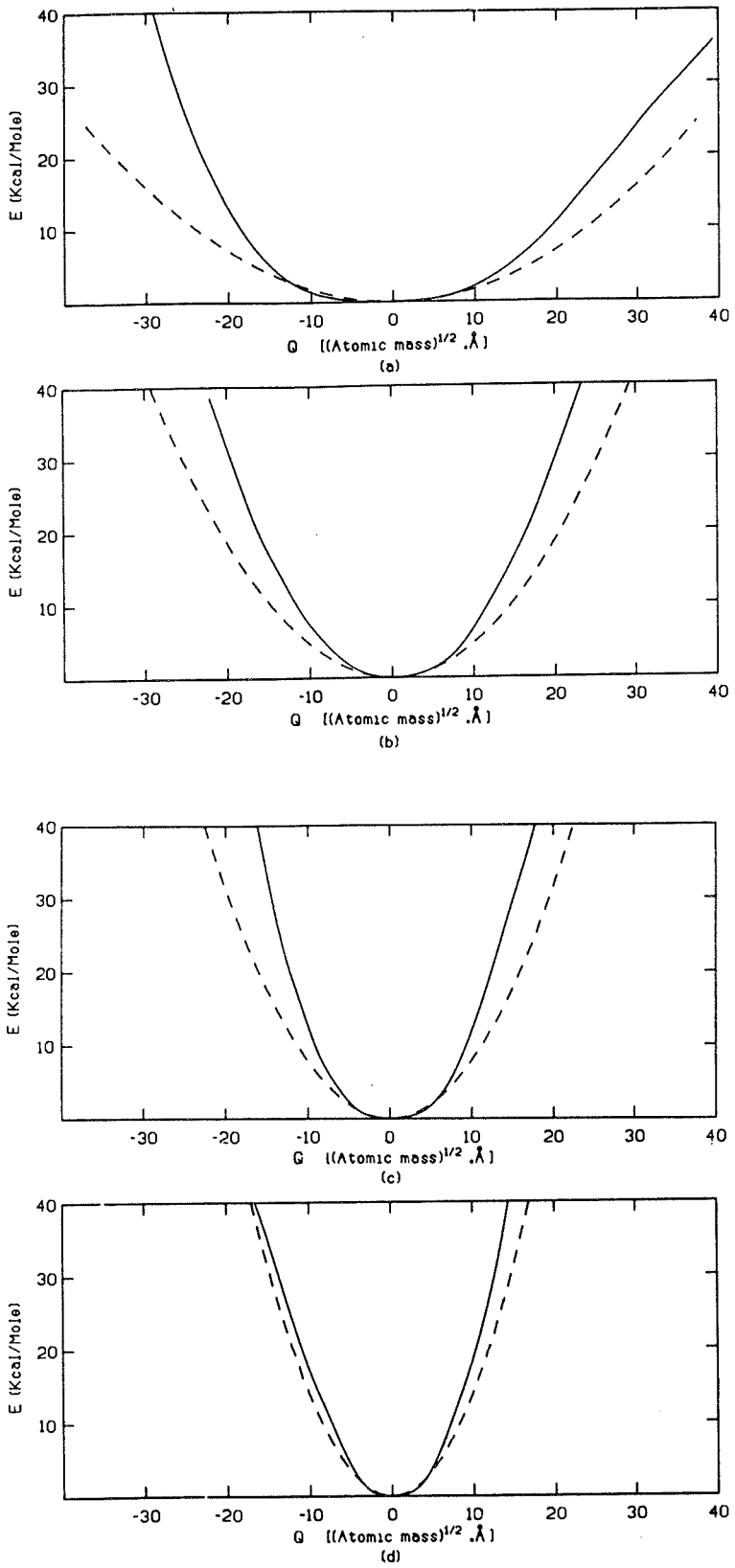

Figure 10. Potential energy along several modes: the solid curve is the total potential energy and the dashed curve corresponds to the harmonic approximation with the zero of energy at the minimum energy conformation. Mass weighted displacements are used. (A displacement of 1 corresponds to approximately 0.3 Å). (a) 14.41 cm^{-1}, (b) 23.45 cm^{-1}, (c) 30.47 cm^{-1}, (d) 40.56 cm^{-1}.

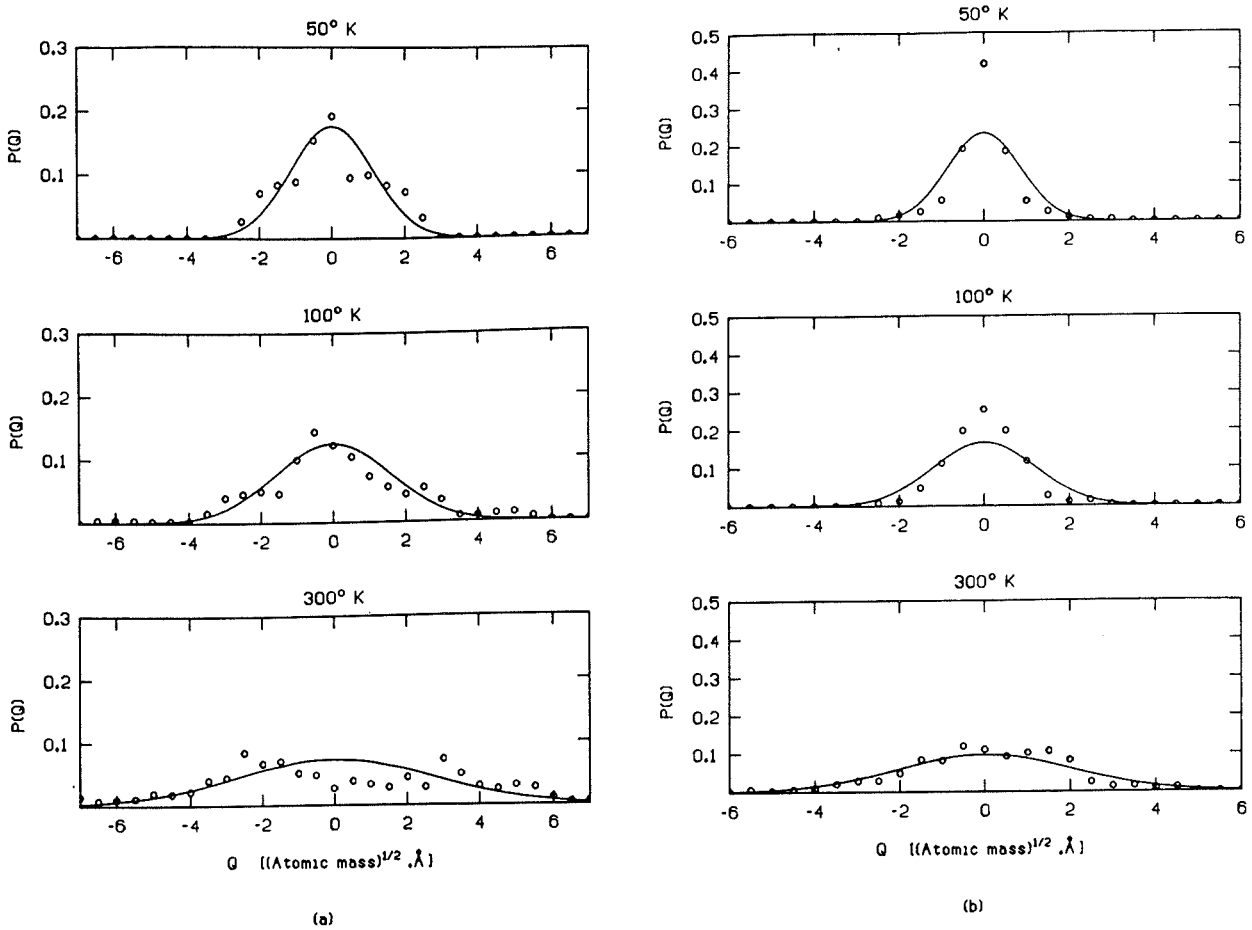

Figure 11. Probability distributions of normal mode coordinates at different temperatures obtained from 20 1-ps trajectories. (a) 30.5 cm^{-1}, (b) 40.6 cm^{-1}, and (c) 81.2 cm^{-1}. Circles correspond to molecular dynamics, and full curves to harmonic case.

jectory are similar. We present results for modes making significant contributions to the atomic displacements. Modes corresponding to frequencies below 30 cm^{-1} have not been included, as they do not have a full period within the 1-ps time interval. Figure 11 shows the probability distributions corresponding to frequencies of 30.5, 40.6, and 81.2 cm^{-1} at 50, 100, and 300 K. The frequency of 81.2 cm^{-1} was included as it is associated with large variations of the ϕ_6 and ψ_6 angles (see the section on anharmonicity in internal coordinates). The harmonic probability distributions are shown for comparison. In general, the molecular dynamics distributions are close to the harmonic distributions in the range of frequencies and temperatures studied. However, the molecular dynamics results are somewhat irregular at 30.5 and 40.6 cm^{-1}, presumably due to the limited sampling from the 1-ps trajectory. At low frequencies and low temperatures (50 and 100 K), the molecular dynamics distributions are more peaked than the corresponding harmonic distributions; at 300 K and 30.5 cm^{-1} the molecular dynamics distribution is flatter than the corresponding harmonic distribution. The molecular dynamics and harmonic distributions at 81.2 cm^{-1} are very close to each other at all the temperatures considered.

It can be concluded from the above results that the harmonic normal modes are a good approximate representation for the collective displacements of atoms, in the range of temperatures from 50 to 300 K.

Time Dependence

Here we analyze the time dependence of Q_j, at various temperatures and different frequencies. The normalized autocorrelations of Q_j obtained from 20 1-ps trajectories are presented in Fig. 12. In

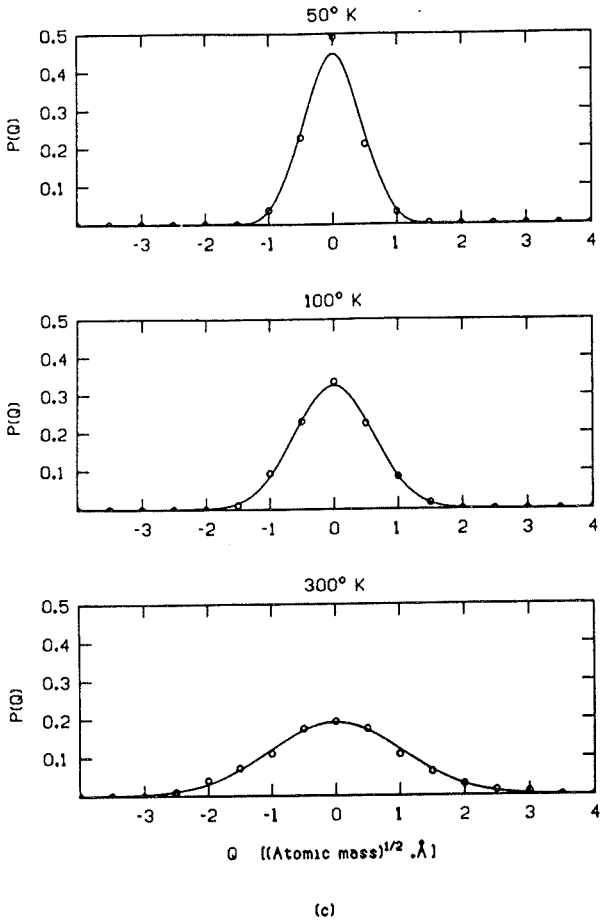

Figure 11. *(Continued from the previous page.)*

general, the loss of correlation at 50 K is small and the decay time is large. At higher temperatures two types of relaxation appear: one concerns the decay of the coarse-grained time average correlation function, and the other concerns the decay of the amplitudes of the oscillations.

The first type of decay is important for high temperatures, although it is also evident at low temperatures. It originates from the coupling of low-frequency oscillations with the higher frequency oscillations under consideration. Such mode mixing is shown in Table V where the dominant frequencies and their amplitudes obtained from the Fourier transform of the autocorrelation functions of Fig. 12 are listed; the mean value of the amplitudes summed over all the spectrum is close to unity. The harmonic frequencies are reproduced with slight shifts within all the range of temperatures studied, but with decreasing amplitude as the temperature increases. Low-frequency modes, especially that close to 44 cm^{-1}, become dominant at 200 and 300 K. The corresponding normalized autocorrelation functions of Q_j from the long trajectory at 300 K are shown in Fig. 13. The mixing of modes is clearly demonstrated because of the longer time interval. The Fourier transform analysis of these autocorrelation functions shows that there are two or three dominant frequencies below 25 cm^{-1} with amplitudes above 0.1, and a multitude of contributions with frequencies between 25 and 300 cm^{-1} with lesser amplitudes. The frequencies close to the harmonic frequencies corresponding to these curves are 1185 cm^{-1} with amplitude 0.018, 253 cm^{-1} with amplitude 0.029, and 168 cm^{-1} with amplitude 0.015, respectively. The comparison of the above results for short and long trajectories shows that mode mixing is more important for the longer trajectory, and that the frequencies close to harmonic frequencies have lesser weights in the long trajectory than in the shorter trajectories. We also notice the appearance of very low-frequency modes (less than 30 cm^{-1}) in the long trajectory (see below), which are not observed in the short trajectories. The decrease of the amplitudes of oscillations with time originates primarily from energy transfer between modes; this affects the amplitudes directly. Similar results have been obtained by molecular dynamics simulations on the lattice dynamics of rare-gas solids, for which the importance of frequency mixing and energy transfers between modes due to the anharmonicity was observed with increasing temperature.[32]

The normalized autocorrelations for some low-frequency modes at 300 K corresponding to the 10-ps molecular dynamics trajectory are presented in Fig. 14, and the corresponding frequencies obtained by Fourier transform are presented in Table VI. It is evident that low-frequency modes make important contributions to the displacements in the 10-ps trajectory. Most significant are the harmonic eigenvectors with frequency below 40 cm^{-1} (e.g., 3 cm^{-1} for the harmonic mode 14.4 cm^{-1}, 17 cm^{-1} for the harmonic mode 23.4 cm^{-1}, and 15 and 25 cm^{-1} for the harmonic mode 30.5 cm^{-1}). Besides this mixing, the molecular dynamics frequency closest to the harmonic frequency has an appreciable contribution (relatively more than for the high-frequency modes), and is dominant for the frequencies of 40.1 and 81.2 cm^{-1} presented here. It has already been shown (Table III) that the effective force constants at 300 K are significantly lower than the harmonic force constants. This is in accord with the finding of low-frequency contributions in the present analysis. The results indicate that much of the anharmonicity is related to low frequencies (below 30 cm^{-1}).

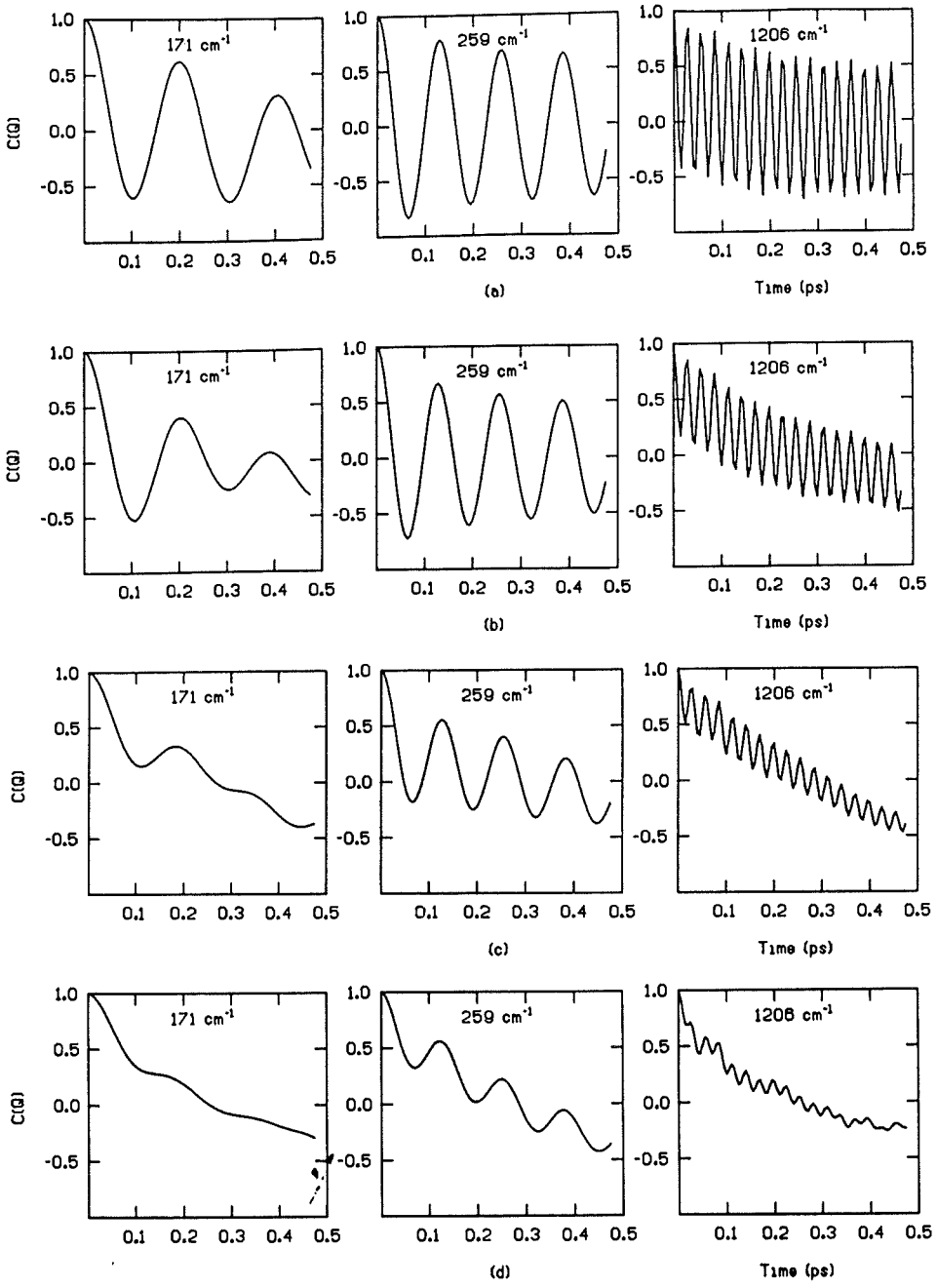

Figure 12. Normalized autocorrelation functions of normal mode coordinate displacements (Q_j) at various temperatures and frequencies, obtained from 20 1-ps trajectories. (a) 50 K, (b) 100 K, (c) 200 K, and (d) 300 K.

Anharmonicity in Internal Coordinates

Mean Square Fluctuations

The rms fluctuations of ϕ, ψ, and ω dihedral angles as a function of residue number obtained from molecular and harmonic dynamics at 5, 100, and 300 K are presented in Fig. 15 and Table VII. The fluctuations of the dihedral angles of the middle residues of the α-helix have almost the same values from molecular dynamics and harmonic dynamics at all the temperatures studied. The rms fluctuations of ϕ of the sixth residue is about 12° by molecular dynamics and 13° by harmonic analysis at 300 K; a value of 15° is found in the 10-ps molecular dynamics trajectory. At the ends of the helix the molecular dynamics values are larger than

Table V Frequencies (in cm^{-1}) Obtained from the Fourier Transform of Normalized Autocorrelation Functions of Fig. 12[a]

Harmonic	50 K	100 K	200 K	300 K
1206	1186(0.65)	1186(0.36)	44(0.52)	45(0.42)
		44(0.34)	132(0.21)	132(0.18)
		128(0.15)	1190(0.17)	203(0.12)
			205(0.13)	348(0.08)
				276(0.07)
				1200(0.07)
				549(0.06)
				424(0.06)
259	264(0.75)	264(0.64)	268(0.40)	44(0.50)
		358(0.17)	40(0.26)	273(0.25)
		168(0.15)	358(0.13)	128(0.18)
		430(0.11)	119(0.11)	195(0.11)
				353(0.11)
171	173(0.59)	182(0.42)	43(0.49)	44(0.50)
		38(0.16)	203(0.25)	129(0.20)
		274(0.15)	128(0.22)	202(0.18)
			280(0.13)	275(0.12)

[a] Only those with amplitudes larger than 0.3, 0.1, 0.05, and 0.05 corresponding to 50, 100, 200, and 300 K, respectively, are listed; the amplitudes are indicated within parentheses (the frequency nearest the corresponding harmonic frequency is underlined).

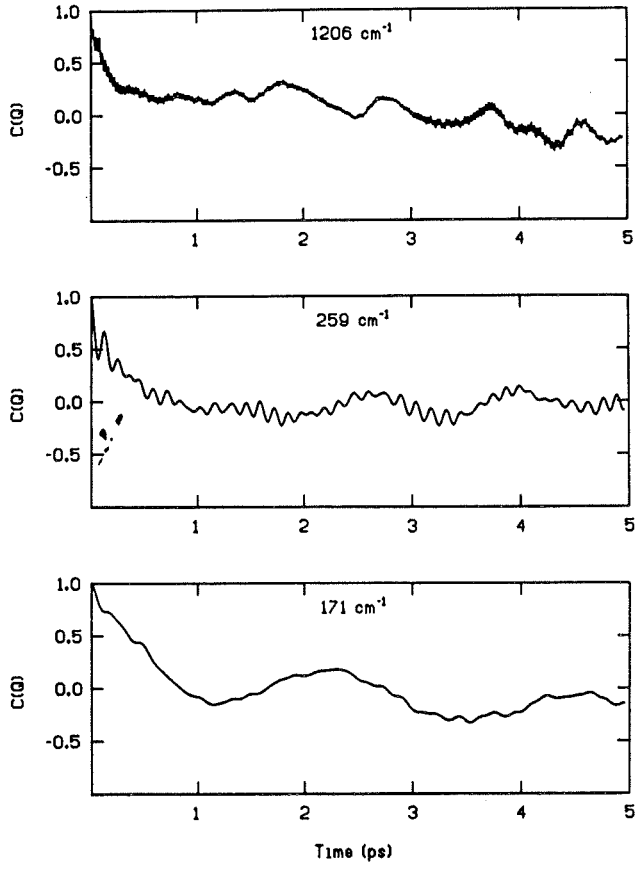

Figure 13. Normalized autocorrelation functions of normal mode coordinate displacements obtained from 10-ps trajectory at 300 K for the frequencies shown in Fig. 12.

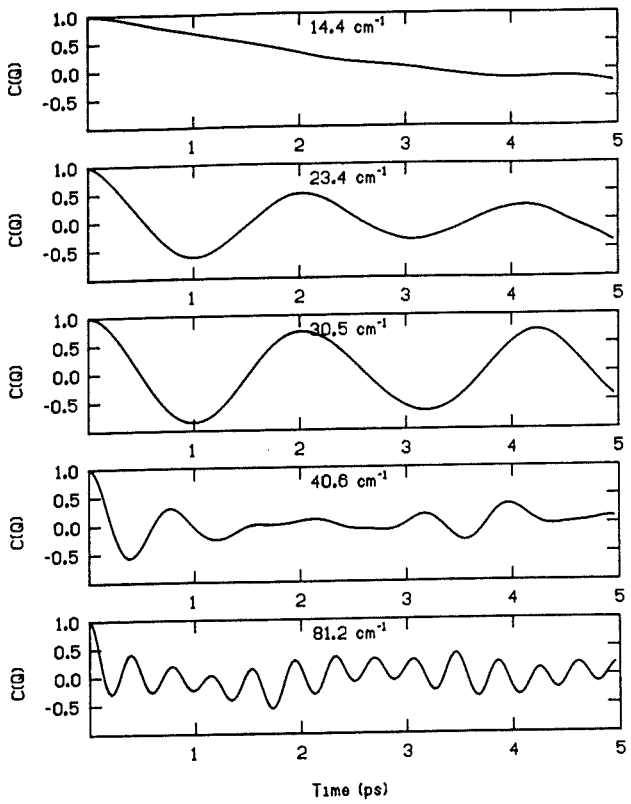

Figure 14. Normalized autocorrelation functions of normal mode coordinate displacements obtained from 10-ps trajectory at 300 K for low-frequency modes.

Table VI Frequencies (in cm^{-1}) Obtained by Fourier Transform of Normalized Autocorrelation Functions of Fig. 14, with Amplitudes Larger than 0.09[a]

Harmonic	Molecular dynamics 300 K	Harmonic	Molecular dynamics 300 K
14.4	3(0.59)	40.6	42(0.20)
	13(0.20)		33(0.17)
	20(0.11)		52(0.14)
	24(0.10)		
23.4	17(0.47)	81.2	87(0.27)
	26(0.16)		12(0.14)
	33(0.11)		68(0.09)
30.5	15(0.74)		
	25(0.25)		
	33(0.13)		
	6(0.13)		
	40(0.10)		

[a]The corresponding amplitudes are indicated within parentheses (the frequency nearest the corresponding harmonic frequency is underlined).

the harmonic results. For ω the fluctuations are smaller than for ϕ and ψ as expected, and the anharmonic effects are even less important. The harmonic behavior of the dihedral angle fluctuations at the middle of the helix at 300 K contrasts with the large anharmonicity observed for the atomic displacements in the same region of the helix.[12] As shown in Fig. 16 and Table VIII, this difference may be accounted for by the fact that there are more high-frequency modes contributing to the dihedral angle fluctuations, as compared with those contributing to the atomic displacements (see Figs. 8 and 9); the corresponding dynamics spectrum, which involves lower frequencies than the harmonic results, is shown in Fig. 7. Anharmonic effects in the atomic displacements at temperatures near 300 K are mainly introduced by low-frequency motions (below 30 cm^{-1}).

Potential of Mean Force

We present in Fig. 17 the potentials of mean force experienced by the angles ϕ, ψ and ω of the middle and end residues of the helix at 300 K. It may be seen that ϕ_6 and ψ_6 fluctuate within harmonic potential wells, while ϕ_1 and ψ_1 fluctuate within potential wells with two minima. These end angles have larger ranges than ϕ_6 and ψ_6 (e.g., ϕ_1 varies from $-70°$ to 110° and ϕ_6 from $-30°$ to 30°). The two minima for the end ϕ and ψ angles suggest that there exist at least two conformational substates at each extremity of the helix. The ω angles fluctuate within a single potential well, with the end angles having a slightly broader potential well than those at the center.

For the central angles the shape of potentials of mean force are almost independent of temperature and they are approximately harmonic.

Time Dependence

Figure 18 shows the short time development of the autocorrelation functions of the dihedral angles ϕ, ψ, ω, and of the improper torsion angles τ(NH) and τ(CO) of the sixth residue. The curves at the left of this figure correspond to a temperature of 5 K and those at the right to 300 K; they are both evaluated from a set of 20 1-ps trajectories. The behavior at the two temperatures is similar, with somewhat less structure at the higher temperature. The fast decay of ϕ, ψ, and ω is in the range of 0.08 ps, while that for τ(NH) and τ(CO) is 0.03 ps. The amplitudes of oscillations observed for the autocor-

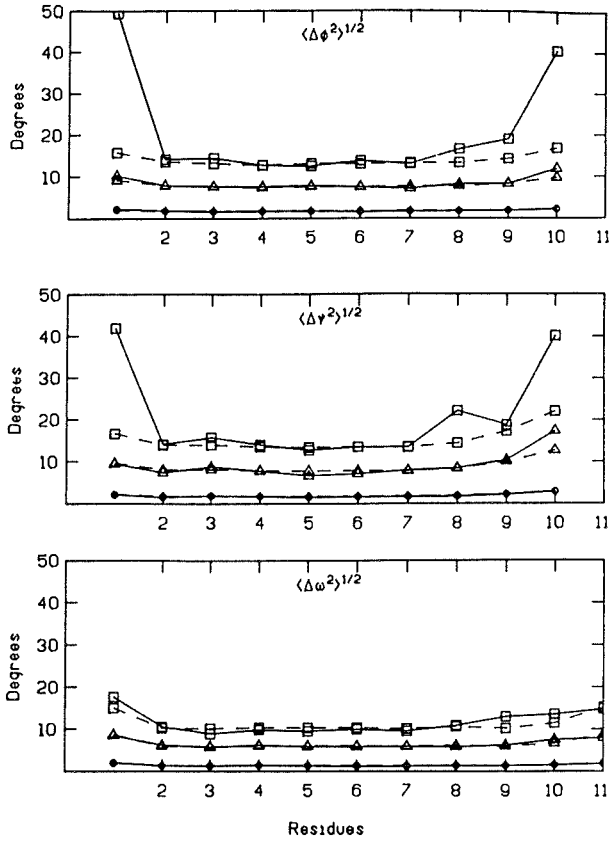

Figure 15. Root mean square fluctuations of ϕ, ψ, and ω dihedral angles obtained from 20 1-ps molecular dynamics at various temperatures (full curves) and the corresponding harmonic values (dashed curves). Circles correspond to 5 K, deltas to 100 K, and squares to 300 K.

Table VII RMS Fluctuations of ϕ, ψ, and ω at Different Temperatures by Molecular and Harmonic Dynamics[a]

	Molecular Dynamics			Harmonic Dynamics		
Temperature	ϕ	ψ	ω	ϕ	ψ	ω
5	1.67	1.69	1.27	1.71	1.84	1.32
100	7.68	8.11	5.92	7.66	8.24	5.92
300	14.64	15.89	10.32	13.26	14.27	10.26

[a]All values in degrees. The fluctuations for a given dihedral angle type are averaged over residues 2–9. The 20 1-ps short trajectories were employed.

relation of τ(NH) decreases significantly between 5 and 300 K. The harmonic autocorrelation functions obtained by Levy et al.[15] in hexadecaglycine for the dihedral angles of the middle residue show a rapid decay of 0.1 ps with a negative excursion and subsequent smaller oscillations; those corresponding to improper torsion angles exhibit well-defined periodic oscillations, with a slow decay. The decays observed in this harmonic analysis are due to dephasing of the normal modes that contribute to the motion of a given dihedral angle. The autocorrelation functions obtained by these authors for the middle residue of the hexadecaglycine are almost identical to those obtained at 5 K for the same angles belonging to the middle residue of decaglycine in the present study. Since there is negligible anharmonicity along normal modes at low temperature (see the section on time dependence), the decay of the autocorrelation functions observed at this temperature is attributable to dephasing. The autocorrelation functions obtained at 300 K are very similar to those at 5 K. Thus, it is likely that the relaxation observed at 300 K is also mainly due to dephasing involving the contributing normal modes. This does not seem to be the case for $\tau(NH)_6$; the fast decay in the amplitude and the frequency change of the oscillations at 300 K, as compared to 5 K, points to the existence of a more complex relaxation mechanism at 300 K.

As compared with the molecular dynamics displacement autocorrelation fluctuations, the decay observed for the dihedral angles has shorter time constants.

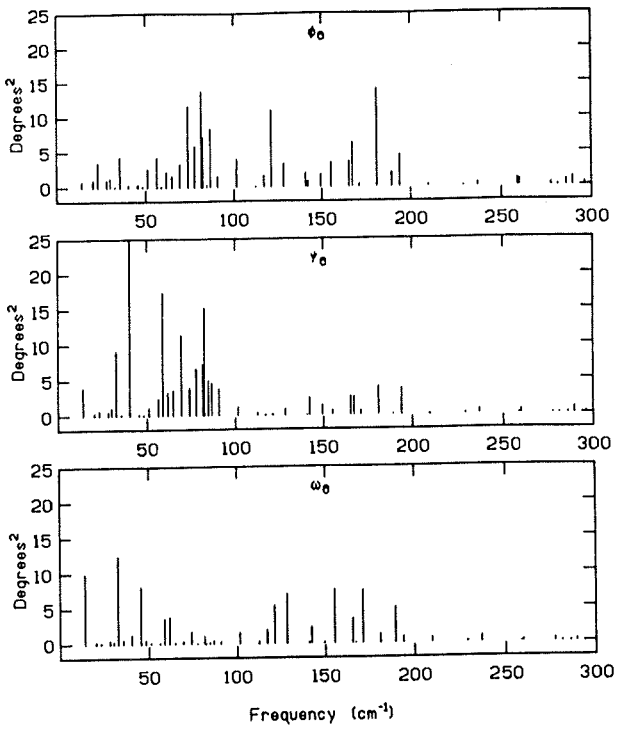

Figure 16. Spectral density of autocorrelation functions of the ϕ, ψ, and ω dihedral angle fluctuations obtained by harmonic analysis.

Heat Capacity

A property of interest is the heat capacity of helices, in particular, and of proteins, in general[33]. Like other thermodynamic properties (e.g., the entropy) for systems with internal degrees of freedom with a wide range of frequencies, quantum corrections play an important role. This contrasts with many dynamical properties (e.g., the atomic displacements), which are dominated by low frequencies and have negligible quantum corrections above 50 K.[12] Thus, the present classical analysis is purely methodological.

The classical heat capacity of the decaglycine helix has been evaluated in two different ways. In the first, the ratio of the increase of the total energy to the corresponding increase of mean temperature has been calculated. This is possible to do because a series of trajectory results at different temperatures is available. As already pointed out in the description of methodology, each trajectory

Table VIII Percentage of Mean Square Atomic Displacements and Mean Square Dihedral Angle Fluctuations Relative to the Sixth Residue of the α-Helix Contributed by Different Sets of Normal Mode Frequencies (300 K)

Range of Frequencies (cm^{-1})	Cartesian Displacements			Dihedral Angles		
	C	O	N	ϕ	ψ	ω
Up to 53	84	53	81	11	28	32
From 55 to 99	13	44	12	35	46	12
Above 111	3	3	7	54	26	56

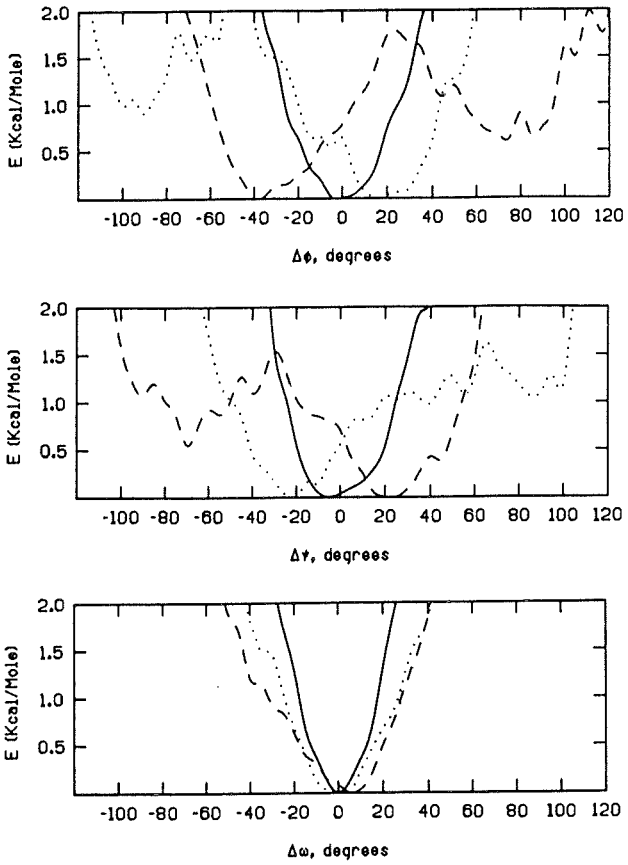

Figure 17. Potential of mean force at 300 K corresponding to ϕ, ψ, and ω dihedral angles of residues in the middle and at the end of the helix, obtained from 20 1-ps molecular dynamics. Full lines correspond to residue 6; dashed lines to first residue, and dotted lines to residue 10.

of a given 20 1-ps set has a constant total energy and a slightly different mean temperature. In Fig. 19 we present the mean temperatures obtained for different sets of trajectories as a function of the total energy. The values of the energy are given with respect to the initial global minimum energy of the system. There is a linear relationship between the total energies and the mean temperatures. Such a linear relationship indicates that the heat capacity is constant over the temperature range studied within the error of the calculation. Further, the heat capacity obtained by taking the slope of the curve is $3k_B$ per atom, where k_B is the Boltzman constant; this is the straight line shown in Fig. 19. Thus, the system is essentially harmonic as far as the classical heat capacity is concerned.

The heat capacity was also computed by considering the fluctuation in the temperature. Most molecular dynamics simulations are done at a single temperature. To obtain the heat capacity from such simulations, in cases where the total energy is fixed (microcanonical ensemble), the fluctuations in the kinetic energy, ΔT, are considered. As shown by Lebowitz et al,[34] one can use the relationship

$$\frac{\langle \Delta T^2 \rangle}{\langle \Delta T \rangle^2} = \frac{2\left(1 - \frac{3}{2C}\right)}{3N} \qquad (10)$$

where N is the number of atoms of the system ($N = 56$) and C the heat capacity. The heat capacity was evaluated for the 10-ps trajectory and for the set of 20 1-ps trajectories at 300 K. The values obtained are 3.24 and 4.23, respectively.

The above results show that the evaluation of the heat capacity from temperature fluctuation is more sensitive to statistical errors than is the evaluation of the average temperature. It depends on good sampling and on the equilibration of the

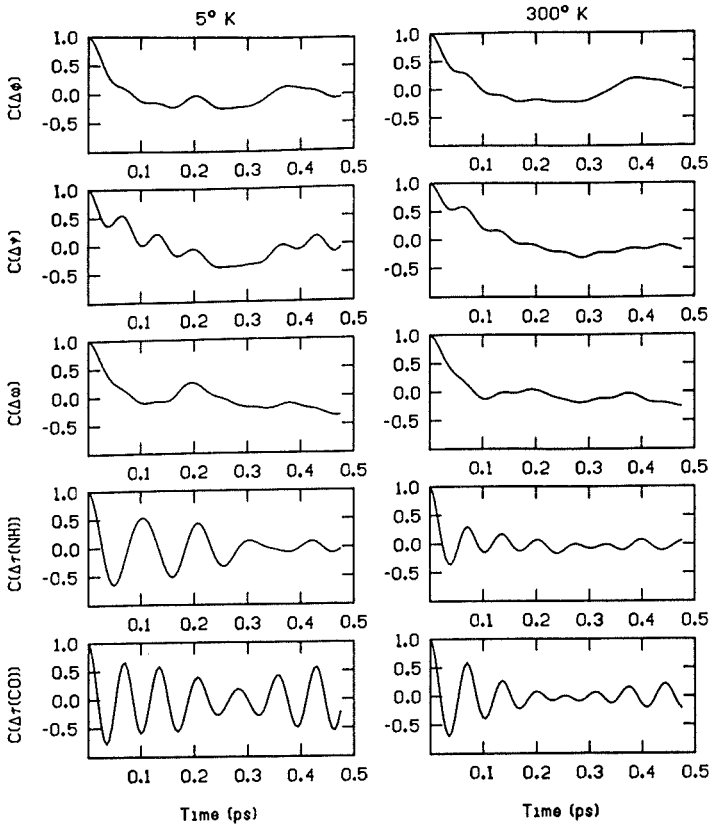

Figure 18. Normalized autocorrelation functions of dihedral angle fluctuations of the sixth residue obtained from 20 1-ps molecular dynamics at 5 and 300 K.

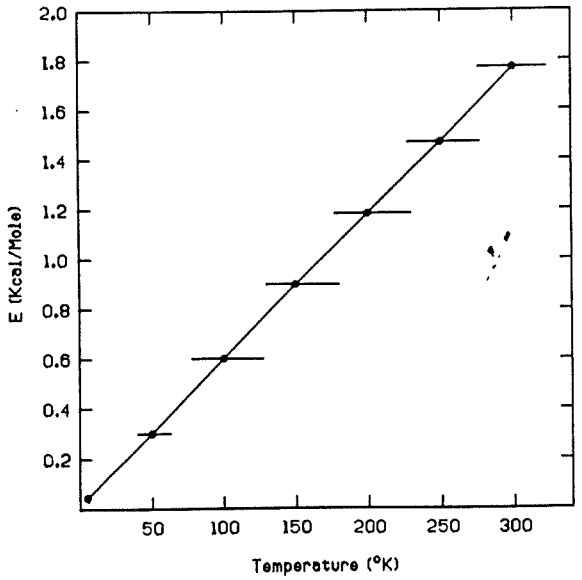

Figure 19. Total energy of the α-helix as a function of mean temperatures obtained from 20 1-ps molecular dynamics trajectories. Dots correspond to mean temperature over 20 trajectories, and bars indicate the range of variation of mean temperatures for a given set of trajectories.

system. The value of the heat capacity computed by Eq. (10) has in fact been used by Dickey and Paskin[32] as a criterion for determining the extent to which a system is equilibrated. The equilibration time for the 10-ps trajectory was 9 ps; for the short trajectories no equilibration time was included after the last kinetic energy input. McCammon, Gelin, and Karplus[3] obtained a value of heat capacity of 2.3 k per atom in a short molecular dynamics simulation of the bovine pancreatic trypsin inhibitor (BPTI). In this 9-ps simulation they considered 7 ps as the equilibration time and only the last 2-ps portion was used for evaluation of the heat capacity. In a more recent molecular dynamics study, McCammon and Karplus[4] found a value of the heat capacity equal to 3.14 k per atom for BPTI. In this simulation the equilibration time was about 85 ps and the final trajectory on which the calculation of the heat capacity was based lasted 96 ps. The present results and the BPTI example demonstrate the importance of having well-preequilibrated dynamical simulations for deriving reliable heat capacity values from temperature fluctuations. Also, it is likely

Table IX Radius of Gyration of the α-Helix and the Components Along the Helix Axis and in the Plane Perpendicular to It at Different Temperatures

Temperature (K)	Radious of Gyration (Å)		
	Total	Axis	Plane
5	10.38	9.66	3.79
50	10.38	9.66	3.79
100	10.37	9.65	3.81
200	10.34	9.60	3.84
300	10.26	9.50	3.88
Minimum energy Configuration	10.37	9.65	3.79

that for the α-helix a longer simulation than 10 ps is required for convergence.

Radius of Gyration

The radius of gyration of the helix has been computed at various temperatures. The values are given in Table IX. The components of the radius of gyration along the axial direction and in the plane perpendicular to the helix axis are given. It may be seen that the total radius of gyration decreases with increasing temperature. The component along the axial direction decreases with temperature while those in the plane perpendicular to the helix

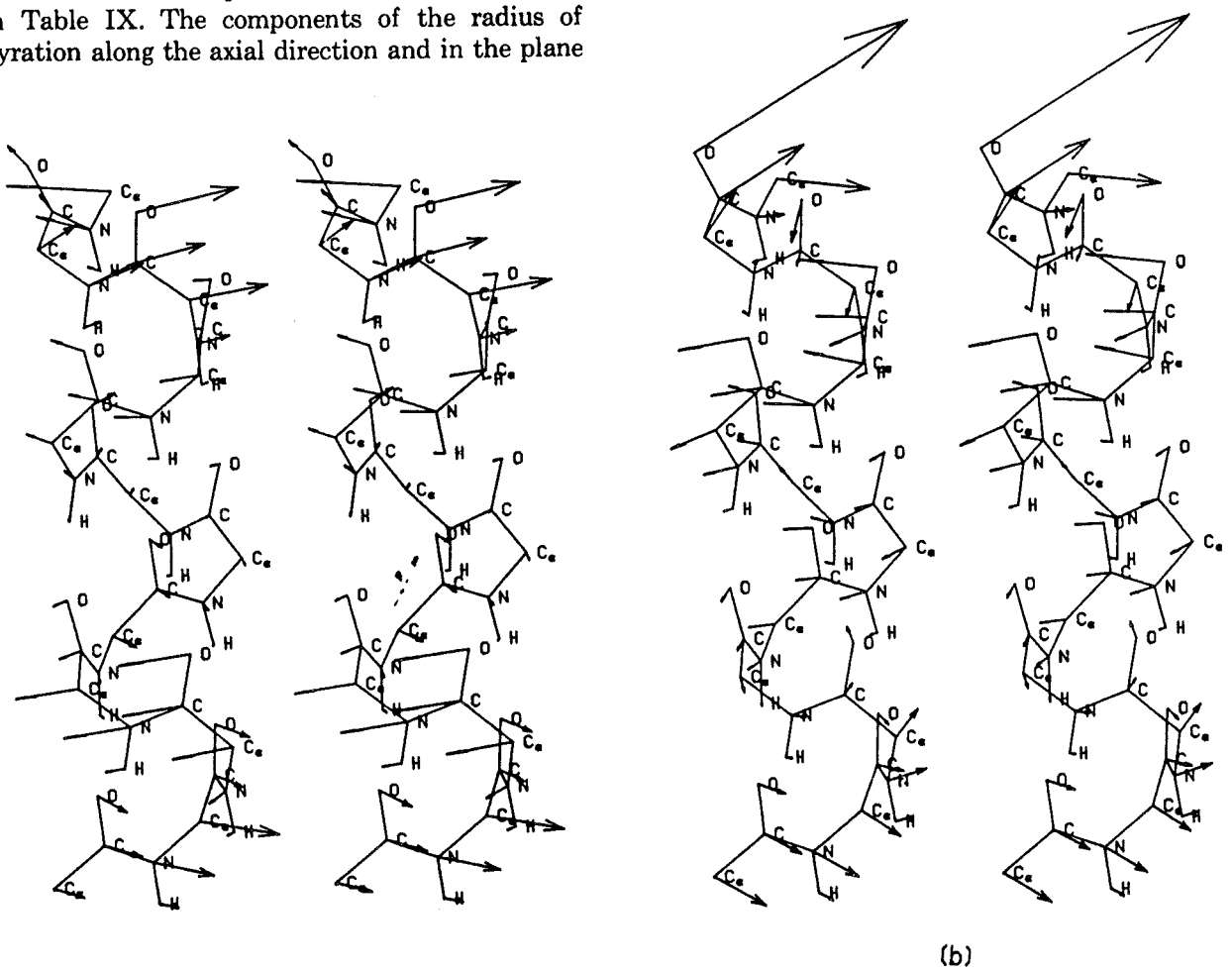

(b)

Figure 20. Stereo views of the α-helix low-frequency modes. The arrows indicate the displacement of each atom in the normal mode (see text). (a) 14.4 cm^{-1}, (b) 20.7 cm^{-1}, (c) 23.4 cm^{-1}, (d) 28.6 cm^{-1}, (e) 30.5 cm^{-1}, (f) 33.1 cm^{-1}, (g) 35.9 cm^{-1}, and (h) 40.6 cm^{-1}.

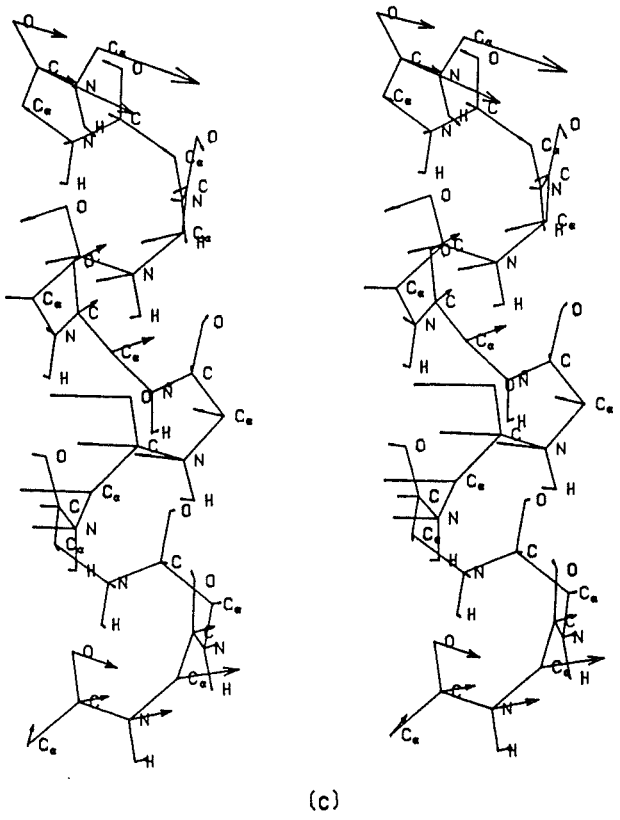

Figure 20. (*Continued from the previous page.*)

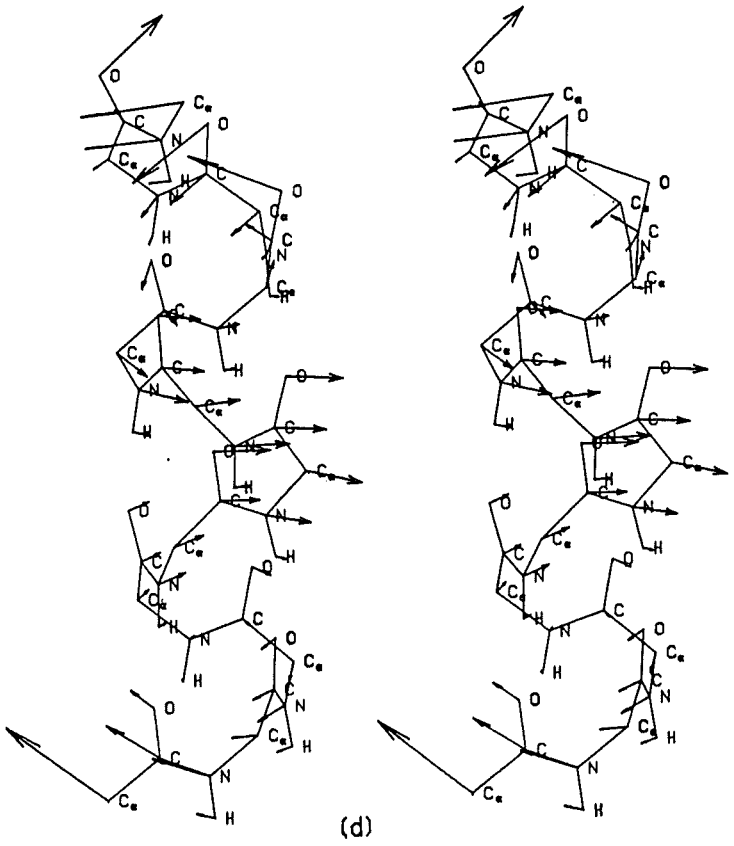

Figure 20. (*Continued from the previous page.*)

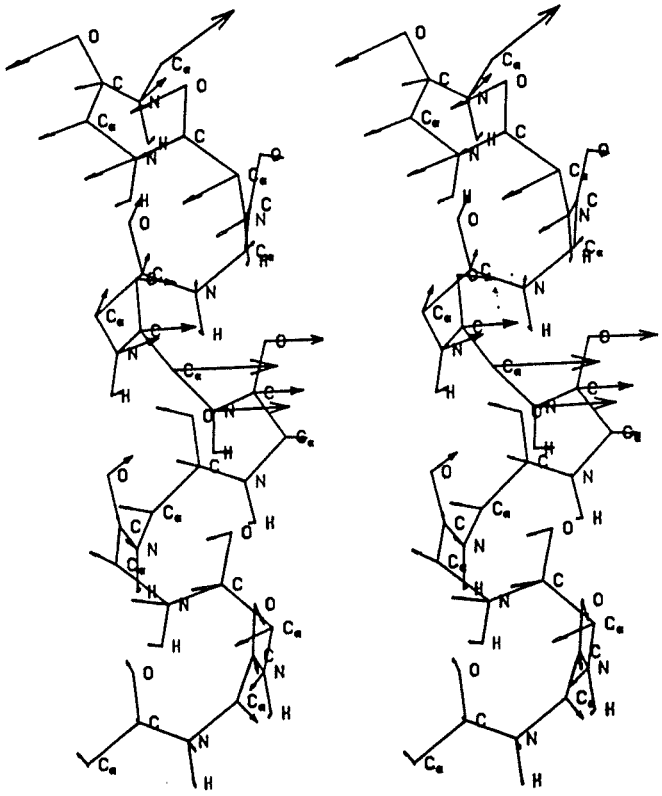

Figure 20. (*Continued from the previous page.*)

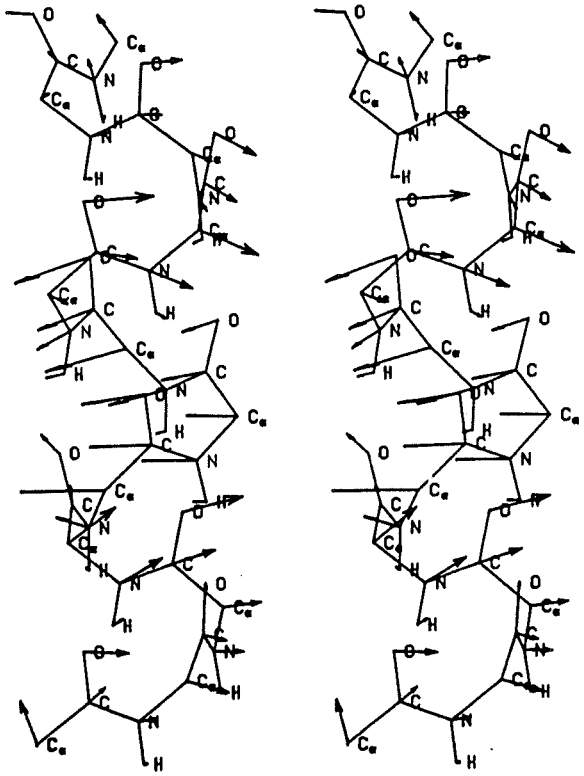

Figure 20. (*Continued from the previous page.*)

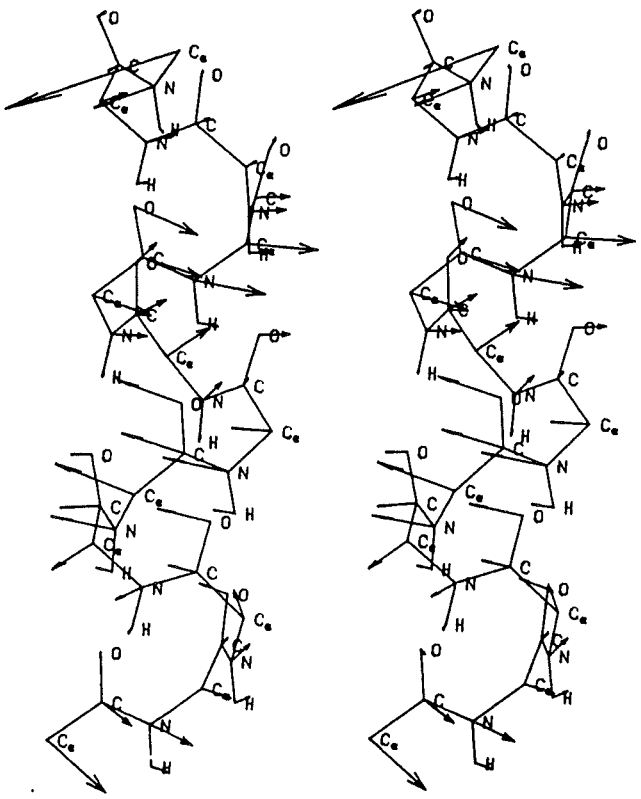

(g)

Figure 20. (*Continued from the previous page.*)

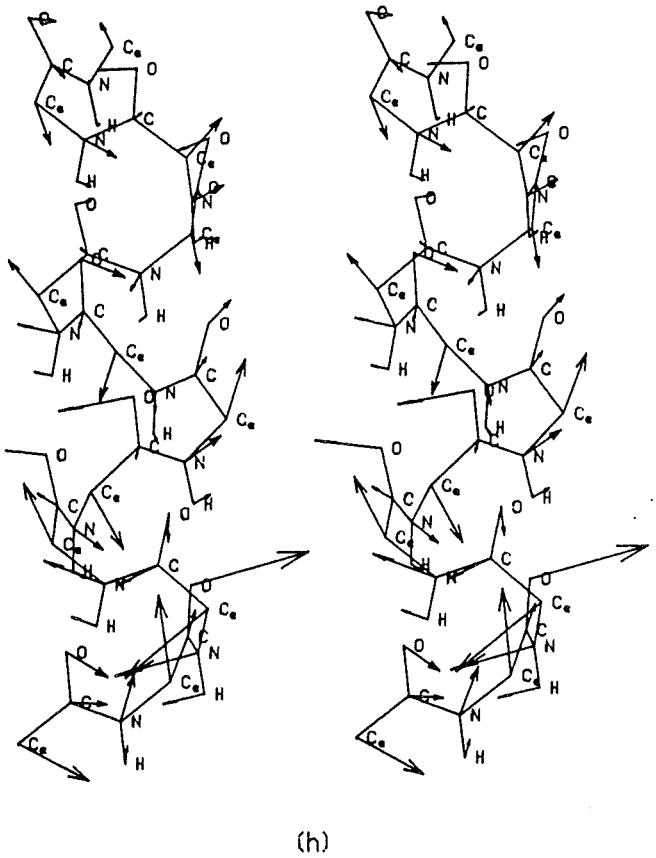

(h)

Figure 20. (*Continued from the previous page.*)

axis increases; i.e., the helix becomes shorter and increases in diameter as the temperature is raised. These results are consistent with the slight thermal contraction of helices observed in x-ray diffraction studies of metmyoglobin at 80 vs 300 K.[23]

Low-Frequency Motions

Since the low-frequency modes dominate the atomic displacements and therefore the distortions of the helix, it is of interest to examine some of the modes in detail. This is particularly true because we have shown that the harmonic model provides a useful first approximation to the dynamics of the α-helix even at temperatures as high as 300 K. We present the form of some of the modes in Fig. 20. The dihedral angle variations and displacements of atoms are calculated by moving the atoms in the direction of the vibrational eigenvector up to a total harmonic potential energy of 2 kcal/mole; the vectors shown in the stereo drawings are obtained by multiplying the displacements by a factor of 10 for clarity.

The vibrational normal mode with frequency 14.4 cm^{-1} [Fig. 20(a)] involves important atomic displacements along the tangential directions at both extremities of the helix. The two ends of the helix have a correlated twisting motion at the frequency considered. The tangential motions are more important than the radial and axial ones for this mode. The normal mode of frequency 20.7 cm^{-1} [Fig. 20(b)] corresponds to a motion where the N-terminal part of the helix opens and closes. The normal mode of frequency 23.4 cm^{-1} [Fig. 20(c)] corresponds to twisting motions of interior portions of the helix between the middle and each of the extremities. The radial components are important throughout the chain and the axial motions are negligible. The normal mode of frequency 28.6 cm^{-1} [Fig. 20(d)] corresponds to a helix bending and twisting at the middle. The normal mode of frequency 30.5 cm^{-1} [Fig. 20(e)] exhibits large atomic displacements in the middle of the helix. They are due to tangential and radial components of atomic displacements. Significant tangential motions occur at both extremities of the helix. The overall motion of the helix corresponds to twist-

ing and a small amount bending in the middle and some twisting at both extremities. The normal mode of frequency 33.1 cm^{-1} [Fig. 20(f)] corresponds to a bend in the middle and twists of interior parts of the helix. The normal mode of frequency 35.9 cm^{-1} [Fig. 20(g)] corresponds to bending and twisting at the interior and N-terminal parts. The normal mode of frequency 40.6 cm^{-1} [Fig. 20(h)] represents an interesting case where the displacements decrease from the CO terminal extremity toward the NH terminal extremity, with most of them in the axial direction; a twisting and bending motion also is evident.

These results suggest that a helix can adopt diverse conformations by deformations along such low-frequency vibrational normal modes. Some of them could be stabilized in the protein interior due to specific interactions, in accord with the observation of a large variety of helical conformations (irregular, curved, or kinked) in the x-ray structures of proteins.[35]

CONCLUSION

A simultaneous molecular and harmonic dynamics analysis has been performed to provide information concerning the nature of the internal motions of α-helices. The direct comparisons of the time-independent and time-dependent quantities evaluated by full molecular dynamics simulations at various temperatures with the corresponding harmonic model results have shown that the importance of the anharmonicity depends on the kind of observable. The rms atomic fluctuations have significant anharmonic components at temperatures above 100 K. This is of importance for crystallographic studies that use the harmonic approximation for the temperature (Debye–Waller) factors. In contrast, the dihedral angle fluctuations, which are relevant for conformational studies, are much closer to being harmonic. These differences in anharmonicity can be explained by the differences in the distribution of normal modes contributing to the fluctuations; i.e., the atomic displacements involve much lower frequencies than the dihedral angle fluctuations.

The analysis of potentials of mean force experienced by individual atoms shows that atomic displacements have approximately Gaussian distributions from 50 to 300 K, with different force constants at each temperature (quasi-harmonic model). At 300 K, the force constants obtained by molecular dynamics are significantly lower than in the harmonic case; this can be explained by mode mixing. The α-helix tangential, radial and axial motions are approximately quadratic with different force constants and different deviations from the anharmonicity in each direction.

The time dependence of the autocorrelation functions shows that the relaxation times for the internal coordinates are much shorter than those for the Cartesian coordinates at 300 K. The spectral analysis confirms the existence of very low-frequency oscillations for the Cartesian displacements that increase the decay time of the autocorrelation functions. The time dependence of the projection of the molecular dynamics displacements on the normal mode coordinates shows that mode mixing is important above 100 K. This accounts in part for the observed anharmonic effects. However, frequencies below the lowest harmonic frequency generated by the full dynamics also make important contributions to the anharmonicity.

We thank S. Swaminathan and B. Brooks for helpful discussions. The calculations reported here were done at Harvard and at CIRCE (France). This work has been supported in part by grants from NATO and the National Science Foundation.

REFERENCES

1. Karplus, M. & McCammon, J. A. (1981) *CRC Crit. Rev. Biochem.* **9**, 293–349.
2. Brooks, C. L., Karplus, M. & Pettitt, B. M. *Proteins, A Theoretical Perspective of Dynamics, Structure, and Thermodynamics* (Adv. in Chem. Phys., Vol. LXXI, Wiley, New York, 1988).
3. McCammon, J. A., Gelin, B. R. & Karplus, M. (1977) *Nature (London)* **267**, 585–590.
4. McCammon, J. A. & Karplus, M. (1980) *Ann. Rev. Phys. Chem.* **31**, 29–45.
5. Frauenfelder, H., Petsko, G. A. & Tsernoglou, D. (1979) *Nature (London)* **280**, 558–563.
6. Artymiuk, P. J., Blake, C. C. F., Grace, D. E. P., Oatley, S. J., Phillips, D. C. & Sternberg, M. J. E. (1979) *Nature (London)* **280**, 563–568.
7. Northrup, S. H., Pear, M. R., McCammon, J. A., Karplus, M. & Takano, T. (1980) *Nature (London)* **286**, 304–305.
8. Swaminathan, S., Ichiye, T., van Gunsteren, W. & Karplus, M. (1982) *Biochemistry* **21**, 5230–5241.
9. Morgan, J. D., McCammon, J. A. & Northrup, S. H. (1983) *Biopolymers* **22**, 1579–1593.
10. McCammon, J. A., Wolynes, P. G. & Karplus, M. (1979) *Biochemistry* **18**, 927–942.
11. Lifshitz, I. M. (1969) *Soviet Phys. JEPT* (Engl. Transl.) 28, 1280–1286.

12. Levy, R. M. Perahia, D. & Karplus, M. (1982) *Proc. Natl. Acad. Sci. USA* **79**, 1346–1350.
13. Karplus, M. & Kushick. J. (1981) *Macromolecules* **14**, 325–332.
14. Levy, R. M., Karplus, M., Kushick, J. & Perahia, D. (1984) *Macromolecules* **17**, 1370–1374.
15. Levy, R. M. & Karplus, M. (1979) *Biopolymers* **18**, 2465–2495.
16. Peticolas, W. L. (1979) *Biopolymers* **18**, 747–755.
17. Go, M. & Co, N. (1976) *Biopolymers* **15**, 1119–1127.
18. Go, N. (1978) *Biopolymers* **17**, 1373–1379.
19. Verlet, L. (1967) *Phys. Rev.* **159**, 98–105.
20. Brooks, B.R., Bruccoleri, R. E., Olafson, B. D., States, D. J., Swaminathan, S. & Karplus, M. (1983) *J. Comput. Chem.* **4**, 187–217.
21. Mao, B., Pear, M. R., McCammon, J. A. & Northrup, S. H. (1982) *Biopolymers* **21**, 1979–1989.
22. Cooley, J. W. & Tukey, J. W. (1965) *Math. Comput.* **19**, 297–301.
23. Hartmann, H., Parak, F., Steigemann, W., Petsko, G. A., Ponzi, D. R. & Frauenfelder, H. (1982) *Proc. Natl. Acad. Sci. USA* **79**, 4967–4971.
24. Keller, H. & Debrunner, P. G. (1980) *Phys. Rev. Lett.* **45**, 68–71.
25. Parak, F., Frolov, E. N., Mossabauer, R. L. & Goldanskii, V. I. (1981) *J. Mol. Biol.* **145**, 825–833.
26. Levy, R. M., Srinivasan, A. R., Olson, W. K. & McCammon, J. A. (1984) *Biopolymers* **23**, 1099–1112.
27. Ichiye, T. & Karplus, M. (1987) *Proteins* **2**, 236–259.
28. Middendorf, H. D. (1984) *Ann. Rev. Biophys. Bioeng.* **13**, 425–451.
29. Gupta, V. D., Boutin, H. & Trevino, S. (1967) *Nature (London)* **214**, 1325–1326.
30. Drexel, W. & Peticolas, W. L. (1975) *Biopolymers* **14**, 715–721.
31. Smith, J., Cusack, S., Pezzeca, U., Brooks, B. R. & Karplus, M. (1986) *J. Chem. Phys.* **85**, 3636–3654.
32. Dickey, J. M. & Paskin, A. (1969) *Phys. Rev.* **188**, 1407–1418.
33. Brooks, B. R. & Karplus, M. (1983) *Proc. Natl. Acad. Sci. USA* **80**, 6571–6575.
34. Lebowitz, J. L., Percus, J. K. & Verlet, L. (1967) *Phys. Rev.* **153**, 250–254.
35. Barlow, D. J. & Thornton, J. M. (1988) *J. Mol. Biol.* **201**, 601–619.

Received February 10, 1988
Accepted December 15, 1988